AURKA destruction is decoupled from its activity at mitotic exit but essential to suppress interphase activity

Ahmed Abdelbaki[1,2], H. Begum Akman[1,2], Marion Poteau[3], Rhys Grant[2,5], Olivier Gavet[3], Giulia Guarguaglini[4] and Catherine Lindon[2]

[1]These authors made equal contributions to the work

[2]Department of Pharmacology, University of Cambridge, Tennis Court Road, CB2 1PD, UK

[3]Institut Gustave Roussy, UMR9019 – CNRS, 114 rue Edouard Vaillant, 94805 Villejuif, France

[4]Institute of Molecular Biology and Pathology, CNR, Via degli Apuli 4, 00185 Roma, Italy

[5]Current address: Department of Biochemistry, University of Cambridge, Tennis Court Road, CB2 1QW, UK

Abstract

Activity of AURKA is controlled through multiple mechanisms including phosphorylation, ubiquitin-mediated degradation, and allosteric interaction with TPX2. Activity peaks at mitosis before AURKA is degraded during and after mitotic exit in a process strictly dependent on APC/C coactivator FZR1. We used FZR1 knockout cells ($FZR1^{KO}$) and a novel FRET-based AURKA biosensor to investigate how activity is regulated in absence of destruction. We found that AURKA activity in $FZR1^{KO}$ cells dropped at mitotic exit as rapidly as in parental cells, despite absence of destruction. Unexpectedly, TPX2 was degraded normally in $FZR1^{KO}$ cells. Overexpression of an N-terminal TPX2 fragment sufficient for AURKA binding, but not degraded at mitotic exit, caused delay in AURKA inactivation. We conclude that AURKA inactivation at mitotic exit is determined not by its own degradation but by degradation of TPX2 and therefore dependent on CDC20 rather than FZR1. The biosensor revealed that FZR1 instead suppresses AURKA activity in interphase and is critically required for assembly of the interphase mitochondrial network after mitosis.

Journal of Cell Science • Accepted manuscript

JCS Advance Online Article. Posted on 11 May 2020

Introduction

Aurora kinase A (AURKA) is a major mitotic kinase required for multiple steps in mitosis, including centrosome maturation, microtubule nucleation and organisation into a bipolar spindle and mitotic checkpoint function (Barr and Gergely, 2007; Courtheoux et al., 2018). Recent studies of the effects of acute inhibition of AURKA during mitosis have concluded that it plays an important role during mitotic exit in regulating assembly of the anaphase spindle upon which sister chromatids are segregated (Hegarat et al., 2011; Lioutas and Vernos, 2013; Reboutier et al., 2013). AURKA also has a number of non-mitotic roles that include disassembly of the primary cilium, regulation of myc family transcription factors and response to replication stress (Buchel et al., 2017; Byrum et al., 2019; Cantor, 2019; Otto et al., 2009; Plotnikova et al., 2012). We and others recently reported that AURKA constitutively regulates mitochondrial morphology and function (Bertolin et al., 2018; Grant et al., 2018) in addition to a previously reported role in promoting mitochondrial fission in mitosis (Kashatus et al., 2011). Given the central role of mitochondrial homeostasis in cell fate and function, this newly identified role for AURKA lends importance to the question of when AURKA is present in the cell cycle, and whether it is active.

Widespread reports in the literature of interphase activity of AURKA, and of its activation through a number of interacting partners (Nikonova et al., 2013), can be explained by the unique allosteric properties of this kinase. Either autophosphorylation of the T-loop (Bayliss et al., 2003; Eyers et al., 2003; Tsai et al., 2003) or allosteric interactors (Dodson and Bayliss, 2012; Levinson, 2018; Ruff et al., 2018; Zorba et al., 2014) contribute to the active conformation of AURKA. The most prominent of these allosteric activators is TPX2, which controls AURKA localization, activation and stability on the mitotic spindle during mitosis (Bayliss et al., 2003; Giubettini et al., 2011; Kufer et al., 2002). Interaction with TPX2, whilst protecting the AURKA autophosphorylated site (pT288 in hsAURKA) from access by PP1 phosphatase (Bayliss et al., 2003), also acts to stabilize the T-loop with or without its phosphorylation. Consequently, phosphatase-mediated reversal of T288 phosphorylation may not be sufficient to eliminate activity of AURKA.

In somatic cells, both AURKA protein and kinase activity are low or undetectable through much of the cell cycle, rising sharply in G2 phase, most prominently on the duplicated centrosomes and then on the bipolar spindle in mitosis. pT288 staining is almost entirely confined to the centrosomes, in line with the idea that autophosphorylation is just one route to activation of AURKA. Indeed a conformational sensor of AURKA detects active kinase on spindle poles as expected but also in the cytoplasm, both during and after mitosis (Bertolin et al., 2016). Mitotic destruction of AURKA begins late in anaphase following assembly of the spindle midzone and at the time of spindle pole disassembly, in a manner that depends on the Cdh1 co-activator (hereafter referred to as FZR1) of the Anaphase Promoting Complex/Cyclosome (APC/C) (Castro et al., 2002; Floyd et al., 2008; Littlepage and Ruderman, 2002; Taguchi et al., 2002).

The APC/C is responsible for destruction of dozens of substrates during mitotic exit and coordinates mitotic exit with the processes of chromosome segregation and cytokinesis through the concerted regulation of its coactivators (Pines, 2011). APC/C-CDC20 initially targets cyclin B and securin during metaphase to drive chromosome segregation and mitotic exit. After anaphase onset altered substrate specificity of APC/C-CDC20 and activation of APC/C-FZR1 together control degradation of the remaining pool of cyclin B (Afonso et al., 2019) as well as other APC/C substrates including Aurora kinases (Lindon et al., 2015). Unlike most substrates, AURKA and AURKB show strict dependence on FZR1 for their destruction in cell-based assays (Clijsters et al., 2013; Floyd et al., 2008; Min et al., 2015). Neither the molecular basis, nor the functional significance of this specificity in AURK targeting, is understood.

Given the complexity of AURKA regulation during the cell cycle, we investigated the contribution of AURKA destruction to its inactivation during mitotic exit using novel tools in the form of a CRISPR/Cas9 FZR1 knockout cell line and a FRET-based AURKA activity biosensor we have recently generated. We conclude from our studies that FZR1-mediated destruction of AURKA plays no role in the timing of its inactivation during mitotic exit but is critical to suppress interphase activity and function of the kinase. We test this idea by demonstrating that reestablishment of mitochondrial connectivity after mitosis requires suppression of activity of undegraded AURKA.

Results

Although AURKA activity has been described to peak in M phase there has been no detailed characterization of how AURKA activity varies through mitosis. In particular the question of how AURKA activity is regulated during mitotic exit, given that AURKA also has anaphase functions (Afonso et al., 2017; Reboutier et al., 2015), and the importance of its ongoing destruction for attenuation of activity, remain unresolved. We first used a commercially available antibody against the activated T-loop of Aurora kinases (pT288 in AURKA) that confirms by immunoblot the peak of active AURKA at mitosis in extracts from synchronised U2OS cells (Figure 1A). We then used the same antibody to stain fixed mitotic cells for immunofluorescence (IF), marking centrosomes with γ-tubulin co-stain. All phospho-epitope signal on the centrosomes and spindle poles was abolished by treatment with AURKA inhibitor MLN8237, whereas the signal at the midbody (where the same antibody recognizes pT232 of AURKB) was insensitive to 100 nM MLN8237, indicating that the centrosomal pT288 signal is specific to AURKA as expected (Figure 1B, Supplementary Figure S1) (Asteriti et al., 2014; de Groot et al., 2015). We quantified fluorescence intensity associated with pT288 at different stages of mitosis scored according to DNA morphology. We found that pT288 was evident at the centrosomes from G2 phase onwards.

Following nuclear envelope breakdown (NEB), prometaphase (PM) cells showed a strong increase in centrosome- and spindle pole- associated pT288 signal, peaking at metaphase. pT288 signal began to decline in anaphase cells before dropping sharply in telophase cells (Figure 1C, D). We concluded that inactivation of AURKA measured as decrease in pT288 signal occurs at approximately the time of onset of AURKA destruction, which occurs around 10 minutes after anaphase onset in human cells (Floyd et al., 2008). We further analysed AURKA inactivation kinetics by immunoblot analysis of extracts from cells synchronized through mitotic exit. Cells were synchronized in mitosis using Eg5 inhibitor STLC to trigger the spindle assembly checkpoint (SAC), then treated with Mps1 inhibitor (AZ3146) to override SAC-mediated mitotic arrest. Immunoblotting of cell extracts shows that under such conditions of 'forced' mitotic exit, cells significantly degrade cyclin B1 – the trigger for anaphase entry - within 15 minutes (Figure 1E). The fall in pT288 and total AURKA levels are delayed relative to cyclin B1 degradation, consistent with events ongoing through anaphase and telophase into following G1 phase.

We investigated whether AURKA destruction contributes to the fall in kinase activity at mitotic exit. Mitotic AURKA destruction is critically dependent on the FZR1 co-activator of APC/C, so we used a FZR1 knockout ($FZR1^{KO}$) in U2OS cells generated by CRISPR/Cas9 (Supplementary Figure S2) to study AURKA inactivation in the absence of its destruction at mitotic exit. Indeed, in $FZR1^{KO}$ cells, AURKA-Venus protein levels measured in single cell degradation assays remained constant after anaphase onset, compared to the parental U2OS cell line (Figure 2A). We further determined that there was no delay in mitotic exit in $FZR1^{KO}$ cells that could account for the stability of AURKA, measuring the elapsed time from anaphase onset to completed DNA de-condensation during unperturbed mitotic exit in parental and $FZR1^{KO}$ U2OS cells expressing H2B-GFP (Figure 2B) or under conditions of forced mitotic exit (Supplementary Figure S2). We found that mitotic exit is in fact slightly accelerated in $FZR1^{KO}$ cells as previously reported using siRNA-mediated suppression of FZR1 (Floyd et al., 2008). We then compared loss of pT288 staining during mitotic exit between parental and $FZR1^{KO}$ cells. We found by immunoblot that loss of pT288 signal was identical in both cell lines despite strong stabilization of the AURKA signal during mitotic exit in $FZR1^{KO}$ cells (Figure 2C, Supplementary Figure S2). AURKB was also stabilized but to a lesser extent, consistent with slower degradation of AURKB (Lindon et al., 2015). We note that degradation of endogenous TPX2 during mitotic exit, like inactivation of AURKA, was insensitive to FZR1 knockout, and appeared more complete in $FZR1^{KO}$ cells, where CDC20 levels persisted compared to the parental cells (Figure 2C). TPX2 was first proposed as a substrate of Cdh1/FZR1-APC/C (Stewart and Fang, 2005) but our results suggest that in an unperturbed mitotic exit TPX2 – like cyclin B1 (CCNB1) – is a substrate for CDC20 ahead of FZR1 activation. We then fixed parental U2OS and $FZR1^{KO}$ cells and processed them for quantitative IF analysis of pT288-AURKA and total AURKA staining at spindle poles at

metaphase and telophase. In this analysis AURKA persisted on spindle poles during mitotic exit in FZR1^{KO} cells compared to parental U2OS (Figure 2D). In both cell lines, active AURKA, as measured by T-loop phosphorylation of the kinase (pT288), was strongly reduced after mitotic exit independent of the residual levels of protein (Figure 2E). We confirmed that the persistence of AURKA on spindle poles is a direct effect of AURKA non-degradation, since wild-type AURKA-Venus, but not a non-degradable version, is rapidly lost from spindle poles in unperturbed mitotic exit (Supplementary Figure S3).

A number of AURKA binding partners have been shown to affect the activity of AURKA, some acting independently of T-loop phosphorylation on T288, via distinct effects on its conformational dynamics. Therefore, we developed a diffusible kinase biosensor, based on the well-established design of a fluorescent protein FRET pair separated by a phospho-threonine binding domain and specific phosphorylation motif (Violin et al., 2003), to provide a cell-wide readout of AURKA activity in living single cells as they progress through mitosis. An AURKA-directed version of FRET biosensor was created using the T210 motif from the T-loop of Plk1 as a well-established target of AURKA (Macurek et al., 2008; Seki et al., 2008). Phosphorylation of the T210 motif in the biosensor causes loss of FRET in mitotic cells, measured as an increase in CFP/YFP emission ratio of approximately 10%, in a manner dependent on its phosphorylation site and sensitive to specific inhibitors of AURKA (Figure 3A-B, Supplementary Figure S4). Some sensitivity to inhibitors of AURKB at higher doses indicated that the biosensor might not be completely specific to AURKA (although selective AURKB inhibitors might also target AURKA at these concentrations) (Supplementary Figure S4). This finding was not unexpected for a diffusible biosensor, since part of the specificity in substrate phosphorylation by Aurora kinases is proposed to reside in the co-localization of kinase with its substrates (de Groot et al., 2015; Hegarat et al., 2011). We then used this biosensor in U2OS and FZR1^{KO} cells to measure Aurora kinase activity at mitosis and following mitotic exit. FRET measurements in mitotic cells were in agreement with the analysis of pT288 staining (Figure 2), in showing that 1/FRET signal started to increase in late G2, peaking after NEB and decaying during mitotic exit and into interphase. We found that the increase in AURKA activity measured at mitotic entry was identical in individual U2OS and FZR1^{KO} cells *in silico* synchronized to NEB. *In silico* synchronization to anaphase onset revealed that the timing of Aurora kinase inactivation was identical (Figure 3D, Supplementary Figure S4), and if FRET signals were normalized to the anaphase onset value, the inactivation curves were directly superimposable (Figure 3E). Therefore, mitotic Aurora kinase inactivation is independent of FZR1-dependent degradation. As shown in Figure 3D, FRET measurements returned to pre-mitotic levels at about 1 hour after anaphase onset, indicating complete inactivation of the mitotic pool of AURKA. We observed, however, that FZR1^{KO} cells built up AURKA activity after mitosis earlier than parental cells and reached a

significantly higher level in G1 phase (Figure 3D). We concluded that destruction of AURKA does not influence its inactivation during mitotic exit but may be important to prevent premature re-activation early in the cell cycle.

How can we explain the timing of AURKA inactivation at mitotic exit? We have previously shown that interaction with TPX2 stabilizes AURKA against APC/C-FZR1-mediated degradation (Giubettini et al., 2011), and from this concluded that loss of interaction with TPX2 contributes to the timing of AURKA degradation at mitotic exit. Our finding here that AURKA degradation plays no role in its inactivation led us to evaluate the hypothesis that AURKA inactivation could in fact depend on TPX2 degradation. One way to test this hypothesis would be through expression of a non-degradable version of TPX2. Since transient overexpression of full-length TPX2 inhibited mitotic progression in our hands, we used an N-terminal fragment of TPX2 (amino acids 1-43) known to be sufficient for binding to and activating AURKA (Bayliss et al., 2003) and not degradable at mitotic exit. We overexpressed TPX2(1-43)-CFP in U2OS and FZR1^{KO} cells and monitored AURKA and pT288-AURKA levels during mitotic exit (Figure 4). We found that persistence of TPX2(1-43) through mitotic exit stabilized AURKA protein in U2OS cells (Figure 4A,B) as previously described (Giubettini et al., 2011). As expected, TPX2(1-43) expression showed no effect on AURKA levels in FZR1^{KO} cells (Figure 4C,D). Importantly, we found a marked effect of TPX2(1-43) in stabilizing the pT288-AURKA signal during mitotic exit in both parental U2OS and FZR1^{KO} cells (Figure 4A-D). We concluded that loss of interaction with TPX2 is the rate-limiting step in inactivation of AURKA at mitotic exit. We also found that inhibition of the candidate phosphatase, PP1, after mitotic exit stabilized pT288 signal (Figure 4E), consistent with the conclusion that de-activation rather than destruction controls AURKA activity during mitotic exit.

If FZR1-mediated destruction of AURKA is not required for its inactivation at mitotic exit, then what is it for? Our FRET recordings revealed a small but significant increase in Aurora kinase activity in FZR1^{KO} cells over parental U2OS cells following mitotic exit (Figure 3D). Using both AURKA biosensor and a previously developed AURKB biosensor (Fuller et al., 2008), and pT288 staining, we examined Aurora kinase activity in cells arrested at the G1/S boundary by double thymidine block. The AURKA biosensor revealed increased Aurora kinase activity in FZR1^{KO} cells that was abolished by treatment with MLN8237 (Figure 5A), but insensitive to low doses of AZD1152 inhibitor (20 - 30 nM) sufficient to abolish AURKB-specific activity (Supplementary Figure S4). Since the AURKB sensor is insensitive to MLN8237 at the dose used (Supplementary Figure S5), we concluded that there is increased AURKA activity in interphase in FZR1^{KO} cells. Consistent with this conclusion, we observed pT288 signal at centrosomes in interphase FZR1^{KO} but not parental U2OS cells (Figure 5B).

Next, we explored how FZR1 affects known AURKA functions in interphase. We and others have previously described a role for AURKA, at physiologically relevant levels of expression, in promoting mitochondrial fission during interphase (Bertolin et al., 2018; Grant et al., 2018), an observation thought to be significant to cellular metabolism given the intimate link between mitochondrial morphology and function (Scott and Youle, 2010). We hypothesized therefore that one consequence of increased interphase AURKA activity in FZR1^{KO} cells should be increased mitochondrial fragmentation, and indeed mitochondrial fragmentation following FZR1 siRNA treatment of HeLa cells has previously been described (Horn et al., 2011). We compared the mitochondrial networks in parental U2OS and FZR1^{KO} cells arrested at the G1/S boundary, when the mitochondria tend to form large interconnected mitochondrial networks (Mitra et al., 2009; Salazar-Roa and Malumbres, 2017). We found that the mitochondrial network is highly fragmented in FZR1^{KO} cells derived from two independent CRISPR/Cas9 clones, and in a manner dependent on AURKA activity (Figure 5C-F, Supplementary Figure S5). We measured reduced mean mitochondrial lengths in FZR1^{KO} cells (Figure 5E), and classified mitochondria according to morphological subtypes, to find a significant increase in the percentage of fragmented globules and significantly reduced tubular morphology in FZR1^{KO} cells (Figure 5F). Horn and co-authors had identified the fission factor dynamin-related protein-1 (DRP1) as the target of FZR1 required for its effect on mitochondrial morphology (Horn et al., 2011). Here we found that inhibition of AURKA activity completely rescued mitochondrial length and morphology in FZR1^{KO} cells (Figure 5E,F, Supplementary Figure S5), consistent with data showing AURKA to be an upstream regulator of DRP1 (Bertolin et al., 2018; Kashatus et al., 2011). By contrast, treatment of FZR1^{KO} cells with an AURKB-specific inhibitor had no effect on mitochondrial length (Supplementary Figure S5). We found no alteration in DRP1 levels in FZR1^{KO} cells (Figure 5G) although, in agreement with (Horn et al., 2011), we observed loss of DRP1 during mitotic exit in parental cells (Figure 5H) and suggest that it could be a substrate for APC/C-CDC20 as well as APC/C-FZR1, or another ubiquitin ligase. We concluded that APC/C-FZR1 regulates mitochondrial dynamics by preventing AURKA reactivation in interphase.

To further test our hypothesis that mitochondrial fragmentation is a direct response to un-degraded AURKA, we tested if the introduction of nondegradable (nd, Δ32-66) versus wild-type (WT) versions of AURKA would show differential effects on mitochondrial dynamics (Figure 6). We used stable RPE1-FRT/TO cell lines expressing either AURKA-Venus-WT or AURKA-Venus-nd under tetracycline control. Induction of AURKA-Venus-WT caused increased mitochondrial fragmentation in unsynchronized cells as previously described (Grant et al., 2018), but AURKA-Venus-nd had a greater effect (Figure 6A,B). Importantly, this mitochondrial phenotype was independent of any effect of AURKA on microtubule dynamics that might contribute to subcellular distribution of mitochondria (Supplementary Figure S6). We then tracked individual cells through mitotic exit in the presence of MitoTracker®. Treatment with MLN8237 interfered with

mitochondrial fragmentation at mitosis as expected from the published findings (Kashatus et al., 2011) (Figure 6C). In the presence of overexpressed AURKA-Venus we found that mitochondria were excessively fragmented as cells progressed out of mitosis into G1 phase, and that this effect was exacerbated in cells expressing AURKA-Venus-nd compared to WT (Figure 6D). We concluded that undegraded AURKA is able to inhibit reassembly of the interphase mitochondrial network, and that AURKA is a direct target of FZR1 in regulating mitochondrial dynamics.

Discussion

AURKA activity increases in preparation for mitosis in parallel with the protein level, and both progressively drop from anaphase onwards. This has led to the expectation that destruction contributes to regulating AURKA activity at mitotic exit (Afonso et al., 2017; Floyd et al., 2008). In this study, however, we found that loss of AURKA activity and destruction of the protein are uncoupled. Lack of the APC/C co-activator FZR1 completely stabilizes AURKA levels but does not affect the timing of AURKA inactivation measured during mitotic exit and into subsequent G1 phase, using pT288 reactivity or a novel FRET biosensor for AURKA activity that we characterise in this study. Therefore, AURKA destruction is not required for timing of its inactivation after mitosis.

Instead we find that FZR1 suppresses AURKA-dependent activity of the FRET biosensor in interphase. In the absence of FZR1 we speculate that the timing of reactivation of AURKA depends on the changing balance of AURKA activators and phosphatases during G1 phase. Although a low level of pT288 is detectable at centrosomes by IF in G1 phase $FZR1^{KO}$ cells, since there are routes to generating active AURKA that do not depend on autophosphorylation (for example under interaction with Nucleophosmin/B23 or TACC3 (Burgess et al., 2015; Reboutier et al., 2012), it is likely that basal AURKA activity in interphase is dependent on AURKA levels in the cell, and is calibrated in each cell cycle by mitotic destruction of the AURKA pool. Such multiple ‘opportunities’ for AURKA activation may underlie the strong association of AURKA overexpression with cancer, particularly where co-overexpressed with an activating partner such as TPX2 (Asteriti et al., 2010), and underscore the importance of ubiquitin-mediated destruction of AURKA in suppressing excess AURKA activity in interphase.

We investigated further the route to inactivation of the mitotic pool of AURKA. We found as expected that pT288 dephosphorylation during mitotic exit could be triggered through loss of interaction with TPX2. TPX2 has been shown to protect AURKA from negative regulation by PP1 (Bayliss et al., 2003; Eyers et al., 2003; Katayama et al., 2001; Tsai et al., 2003). Indeed, whereas PP6 has been shown to act on the AURKA-TPX2 complex to limit AURKA activity in spindle assembly, PP1 can act only on ‘free’ AURKA (Zeng et al., 2010). We found that

overexpression of the TPX2 (1-43) peptide that is sufficient to activate AURKA, and which is not degraded at mitotic exit, delayed the timing of kinase inactivation.

Our data indicate that the 'release' of AURKA to PP1-mediated inactivation could depend on APC/C-CDC20-mediated destruction of TPX2. We cannot exclude that ubiquitination of TPX2 would be enough to abrogate interaction, or that loss of interaction would be an indirect consequence of APC/C-CDC20 activity. However, our idea is consistent with the early degradation of TPX2 that we observe, and studies indicating TPX2 as a major substrate for APC/C at mitotic exit (Min et al., 2014; Singh et al., 2014) and numerous observations that amplification of TPX2 is the rate-limiting event for increased AURKA activity associated with tumorigenesis (Asteriti et al., 2010; Shah et al., 2019). One interesting conclusion to be drawn from our model is that although AURKA destruction during mitotic exit is a FZR1-dependent event, AURKA inactivation during mitotic exit is dependent on CDC20, along with all of the other known critical events of mitotic exit. This helps to explain why mitotic exit occurs essentially normally in absence of FZR1. Indeed, FZR1 is not expressed during early embryonic cell cycles, and AURKA activity regulated by activation and inactivation, instead of periodic proteolysis (Littlepage and Ruderman, 2002). Throughout development AURKA destruction therefore remains 'decoupled' from mitosis in a manner that contrasts with most other substrates of APC/C-FZR1, that can also be targeted by APC/C-CDC20 (Lindon et al., 2015). We infer that the unusual relationship between APC/C and Aurora kinases preserves a pool of potential Aurora kinase activity with critical interphase functions, regulatable through proteostasis.

So, what are the FZR1-sensitive AURKA-dependent events of interphase? Previous studies have shown that AURKA activity acts as an upstream regulator of mitochondrial morphology through RALA-dependent and -independent pathways (Bertolin et al., 2018; Kashatus et al., 2011). Mitochondria are highly dynamic organelles that undergo constant fission and fusion to modulate connectivity of the mitochondrial network, allowing the cell to respond to metabolic demands and maintain a healthy mitochondrial network. Increased rates of fission occur in preparation for mitosis so that mitochondrial fragments can be equally distributed between daughter cells and reassembly of the mitochondrial network is a critical step in the post-mitotic reconstitution of the interphase state. Here we show that the presence of non-degraded AURKA delays reassembly of the mitochondrial network after cell division. Whilst there is increasing evidence that the dynamic state of mitochondria contributes to the overall metabolic state of the cell, our understanding of how this impacts progression in the cell cycle remains limited (Mitra et al., 2009; Salazar-Roa and Malumbres, 2017). Our study provides new evidence that APC/C-FZR1 control of AURKA activity in interphase is a critical parameter in regulation of mitochondrial dynamics.

Materials and Methods

Generation of U2OS FZR1$^{-/-}$ knockout cell line (FZR1^{KO})

Two guide RNAs (GACGTCCGATTGGAACGGCG and GCCCTGCCTCGCCATGGACC) targeting the first exon of FZR1 were cloned into AIO-GFP nickase vector, a gift from Steve Jackson (Addgene plasmid # 74119) (Chiang et al., 2016).

U2OS cells were transfected with 2 µg of plasmid by electroporation using the Neon Transfection System according to the manufacturer's instructions (Thermo Fisher Scientific). 48 hours after transfection cells were sorted based on GFP into 96-well plates at a single-cell-per-well density for clonal expansion. Single-cell clones were validated for loss of FZR1 by sequencing the genomic locus, immunoblotting and live-cell imaging of APC/C substrates. We tested that U2OS parental and FZR1^{KO} cells have identical DNA content and are mycoplasma-free.

Cell culture, synchronization and drug treatments

U2OS and FZR1^{KO} cells were cultured in DMEM (Thermo Fisher Scientific) supplemented with 10% FBS, 200 µM Glutamax-1, 100 U/ml penicillin, 100 µg/ml streptomycin, and 250 ng/ml fungizone at 37°C with 5% CO2. For mitotic exit synchronizations, cells were collected in mitosis by 12 h treatment with 10 µM STLC (Tocris Bioscience) to trigger the Spindle Assembly Checkpoint (SAC) and then released by treatment with 10 µM AZ3146 (Generon, Slough, UK), an inhibitor of the SAC kinase Mps1. Cells were synchronized at other cell cycle stages as follows: For G0, cells were starved for 48 h in DMEM without serum. For G1, G0-arrested cells were released into serum-containing media for 2 h. For G1/S, cells were incubated with media containing 2 mM thymidine for 16 h, washed with PBS, released into regular media for 12 h, and then incubated in media containing 2 mM thymidine for 15 h. S-phase cells were prepared by releasing G1/S phase cells into regular media minus thymidine for 5 h. For M-phase cell population, cells were incubated with 10 µM STLC for 12 h. Mitotic cells were then collected by shake-off.

Aurora kinase inhibitors MLN8237 (Stratech, Ely, UK), MK5108 (Axon Medchem, Groningen, Netherlands), ZM447439 (Generon) and AZD1152-HPQA (Sigma-Aldrich UK) were used at the doses indicated.

RPE-1 cells, and RPE-1 FRT/TO cell lines expressing AURKA-Venus and AURKA-nd-Venus were cultured as previously described (Grant et al., 2018).

Plasmids and transient transfection

pVenus-N1-AURKA, AURKA-Δ32-66 (Floyd et al., 2008; Littlepage and Ruderman, 2002) and TPX2(1-43) (Giubettini et al., 2011) have been described in the publications cited.

The non-targeted AURKB FRET biosensor was a kind gift from Michael Lampson (Fuller et al., 2008).

The AURKA-directed FRET biosensor was created as followed: We modified a FRET construct backbone containing mTurquoise and mVenus sequences in the pECFP-C1 Clontech vector (construct "F36" (Piljic et al., 2011), a kind gift from Carsten Schultz). First, mVenus was replaced by YPet sequence using KpnI and BamHI restriction sites. The sequence of the FHA2 domain from ScRad53 was amplified by PCR and inserted between AgeI and MluI sites, introducing HindIII and EcoRI sites upstream of MluI. Finally, complementary oligonucleotides encoding the phosphorylation site Thr210 of Plk1 were annealed and inserted between EcoRI and MluI sites. Amino acid sequence used: NH_2-*G*-*G*-*S*-*G*-*G*-K-V-Y-D-G-E-R-K-K-K-**T**-L-C-I-COOH. Note that an isoleucine was introduced at the +3 position for FHA2 binding. The final plasmid construct contains the following elements: NcoI-mTurquoise-BglII-AgeI-FHA2-HindIII-EcoRI-Plk1 T210 phosphorylation sequence-MluI-YPet-BamHI. Complete sequence is available upon request.

Cells were transfected using electroporation with Neon Transfection System (Invitrogen™) using the following parameters: pulse voltage 1500 V, pulse width 10 ms, and 2 pulses total on the transfection device according to the manufacturer's protocol.

Immunoblotting

Cells were lysed in in 1% Triton X-100, 150 mM NaCl, 10 mM Tris–HCl at pH 7.5 and EDTA-free protease inhibitor cocktail (Roche), and PhosSTOP™ inhibitor for phosphatase (Sigma-Aldrich). After 30 min on ice, the lysate was centrifuged at 14,000 rpm (4°C) for 10 min. For immunoblotting, an equal amount of protein (20 µg) were loaded into SDS-PAGE 4-12% pre-cast gradient gels. Proteins were transferred to Immobilon-P or Immobilon-FL membranes using the XCell IITM Blot Module according to the manufacturer's instructions. Membranes were blocked in PBS, 0.1% Tween-20, 5% BSA and processed for immunoblotting. Primary antibodies for immunoblot were as follows: AURKA mouse mAb (1:1000; Clone 4/IAK1, BD Transduction Laboratories), phospho-Aurora A (Thr288)/Aurora B (Thr232)/Aurora C (1:1000; clone D13A11 XP® Rabbit mAb, Cell Signalling), rabbit polyclonal TPX2 antibody (1:1000; Novus Biological), Cdh1 mouse mAb (1:50; gift from T. Hunt and J. Gannon), CDC20 mouse mAb (1:1000; Santa Cruz sc13162), AURKB rabbit polyclonal antibody (1:1000; Abcam ab2254), mouse monoclonal Cyclin B1 (1:1000; BD 554177), DRP1 rabbit polyclonal (1:500; Bethyl lab), rabbit polyclonal Tubulin (1:2000; Abcam ab6046), mouse mAb anti-Vinculin (1:1000; clone hVIN-

1, Sigma-Aldrich), rabbit anti-GFP (1:1000; 11814460001, Roche). Secondary antibodies used were HRP-conjugated, or IRDye® 680RD- or 800CW-conjugated at 1:10000 dilution for quantitative fluorescence measurements on an Odyssey® Fc Dual-Mode Imaging System (LICOR Biosciences). Quantitative immunoblotting was carried out using IRDye® 680RD and 800CW fluorescent secondary antibodies, scanned on an Odyssey® Imaging System (LI-COR Biosciences).

Immunofluorescence analysis

Cells were seeded at 2 x 10^4 onto glass coverslips and then fixed with cold 100% methanol (−20°C), permeabilized with 0.5% Triton X-100 in PBS, and incubated in 2% bovine serum albumin (BSA), 0.2% Triton X-100 in PBS (blocking buffer) for 1 h at room temperature. Cells were incubated overnight with primary antibodies (rabbit phospho-AURKA Thr288, 1:50; mouse anti-γ-tubulin GTU-88, Sigma-Aldrich; 1:1000) diluted in blocking buffer at 4°C, then washed three times with blocking buffer and incubated with secondary antibodies at 1:1000 dilution. Alexa Fluor 488 anti-mouse and Alexa Fluor 568 anti-rabbit (Thermo Fisher Scientific) were used as the secondary antibodies. DNA was stained with DAPI. Coverslips were mounted with Prolong Gold antifade reagent. Epifluorescent stacks were acquired using 500 nm step with 2×2 bin using appropriate filter sets and 40X NA 1.3 oil objective. The best in-focus images were selected and integrated intensities were measured by ImageJ (http://rsb.info.nih.gov/ij/; National Institutes of Health, Bethesda, MD).

Mitochondrial imaging and analysis

Cells were seeded at 2 × 10^4 onto eight-well plastic-bottom slides (Ibidi GmbH, Martinsried, Germany) for live cell imaging. To stain the mitochondria, the cells were incubated with 100 nM Mitotracker® Red CMXRos (M7512, Thermo Fisher Scientific) for 15 min, which was then replaced with L-15 medium supplemented with FBS. Epifluorescent images were acquired with 40X NA 1.3 oil objective on an Olympus IX81 motorized inverted microscope (Olympus Life Science, Southend-on-Sea, UK). The automated imaging platform included PE4000 LED illumination source (CoolLED, Andover, UK), Retiga R6 CCD camera (QImaging, Birmingham, UK), motorized stage (Prior Scientific, Cambridge, UK) and 37°C incubation chamber (Solent Scientific, Segensworth, UK), all controlled by Micro-Manager (Edelstein 2014). Images were collected with 2x2 bin applied, exported as tiff files and analysed using MicroP (Grant et al., 2018; Peng et al., 2011). In mitochondrial length analyses each datapoint represents the mean value of 30 mitochondrial fragments per cell.

Timelapse imaging and FRET quantification

Cells were imaged in L-15 medium with 10% FBS at 37°C using an automated epifluorescence imaging platform composed of Olympus IX83 motorized inverted microscope, Spectra-X multi-

channel LED widefield illuminator (Lumencor, Beaverton, OR, USA), Optospin filter wheel (Cairn Research, Faversham, UK), CoolSnap MYO CCD camera (Photometrics, Tuscon, AZ, USA), automated XY stage (ASI, Eugene, OR, USA) and climate chamber (Digital Pixel, Brighton, UK) and controlled using Micro-Manager. FRET imaging was performed using a 40X NA 0.95 objective and ECFP/EYFP/mCherry beamsplitter (Chroma, Bellows Falls, VT, USA) for ratiometric comparison of CFP and YFP emission upon excitation of CFP. ImageJ software (National Institutes of Health) was used to quantify CFP and YFP signal across the whole cell and AURKA activity expressed as CFP/YFP ratio (1/FRET).

Statistical Analysis

Data analyses were performed in GraphPad 6.01 (San Diego, CA, USA). Results were analyzed with Student's t-test or Mann-Whitney U-test (non-parametric) as indicated in figure legends. Significant results are indicated as $p < 0.05$ (*), $p \leq 0.01$ (**) or $p \leq 0.001$(***). Values are stated as the mean ± standard deviations.

Acknowledgements

The authors thank Steve Jackson's lab for the gift of AIO-GFP plasmid, Carsten Schultz for plasmid F36 and Michael Lampson for AURKB biosensor. We are grateful to Chiara Marcozzi for her advice on CRISPR/Cas9 and to Lilia Gheghiani for the design of FRET constructs. This work was funded by the MRC (MR/M01102X/1) and a Yousef Jameel Scholarship from the Cambridge International Trust to AA. OG is funded by Agence Nationale de la Recherche (ANR-15-CE13-0001) and GG by the Italian Association for Cancer Research (AIRC IG-17390). CL and GG acknowledge support from a Royal Society International Exchanges Award (IES/R3/170195).

Author contributions

Project was conceived by CL, devised by CL, AA & HBA and carried out by AA whilst HBA created and characterized $FZR1^{KO}$ cells and contributed experiments in Figure 2. MP carried out characterization of FRET biosensor (Figures 3 and S4). RG contributed experiments shown in Figures 6 and S6. Manuscript was written by AA & CL, results and manuscript discussed by all authors.

Conflict of interest

The authors declare no competing financial interests.

References

Afonso, O., Castellani, C. M., Cheeseman, L. P., Ferreira, J. G., Orr, B., Ferreira, L. T., Chambers, J. J., Morais-de-Sa, E., Maresca, T. J. and Maiato, H. (2019). Spatiotemporal control of mitotic exit during anaphase by an aurora B-Cdk1 crosstalk. *Elife* **8**.

Afonso, O., Figueiredo, A. C. and Maiato, H. (2017). Late mitotic functions of Aurora kinases. *Chromosoma* **126**, 93-103.

Asteriti, I. A., Di Cesare, E., De Mattia, F., Hilsenstein, V., Neumann, B., Cundari, E., Lavia, P. and Guarguaglini, G. (2014). The Aurora-A inhibitor MLN8237 affects multiple mitotic processes and induces dose-dependent mitotic abnormalities and aneuploidy. *Oncotarget* **5**, 6229-42.

Asteriti, I. A., Rensen, W. M., Lindon, C., Lavia, P. and Guarguaglini, G. (2010). The Aurora-A/TPX2 complex: a novel oncogenic holoenzyme? *Biochim Biophys Acta* **1806**, 230-9.

Barr, A. R. and Gergely, F. (2007). Aurora-A: the maker and breaker of spindle poles. *J Cell Sci* **120**, 2987-96.

Bayliss, R., Sardon, T., Vernos, I. and Conti, E. (2003). Structural basis of Aurora-A activation by TPX2 at the mitotic spindle. *Mol Cell* **12**, 851-62.

Bertolin, G., Bulteau, A. L., Alves-Guerra, M. C., Burel, A., Lavault, M. T., Gavard, O., Le Bras, S., Gagne, J. P., Poirier, G. G., Le Borgne, R. et al. (2018). Aurora kinase A localises to mitochondria to control organelle dynamics and energy production. *Elife* **7**.

Bertolin, G., Sizaire, F., Herbomel, G., Reboutier, D., Prigent, C. and Tramier, M. (2016). A FRET biosensor reveals spatiotemporal activation and functions of aurora kinase A in living cells. *Nat Commun* **7**, 12674.

Buchel, G., Carstensen, A., Mak, K. Y., Roeschert, I., Leen, E., Sumara, O., Hofstetter, J., Herold, S., Kalb, J., Baluapuri, A. et al. (2017). Association with Aurora-A Controls N-MYC-Dependent Promoter Escape and Pause Release of RNA Polymerase II during the Cell Cycle. *Cell Rep* **21**, 3483-3497.

Burgess, S. G., Peset, I., Joseph, N., Cavazza, T., Vernos, I., Pfuhl, M., Gergely, F. and Bayliss, R. (2015). Aurora-A-Dependent Control of TACC3 Influences the Rate of Mitotic Spindle Assembly. *PLoS Genet* **11**, e1005345.

Byrum, A. K., Carvajal-Maldonado, D., Mudge, M. C., Valle-Garcia, D., Majid, M. C., Patel, R., Sowa, M. E., Gygi, S. P., Harper, J. W., Shi, Y. et al. (2019). Mitotic regulators TPX2 and Aurora A protect DNA forks during replication stress by counteracting 53BP1 function. *J Cell Biol* **218**, 422-432.

Cantor, S. (2019). TPX2 joins 53BP1 to maintain DNA repair and fork stability. *J Cell Biol* **218**, 383-384.

Castro, A., Arlot-Bonnemains, Y., Vigneron, S., Labbe, J. C., Prigent, C. and Lorca, T. (2002). APC/Fizzy-Related targets Aurora-A kinase for proteolysis. *EMBO Rep* **3**, 457-62.

Chiang, T. W., le Sage, C., Larrieu, D., Demir, M. and Jackson, S. P. (2016). CRISPR-Cas9(D10A) nickase-based genotypic and phenotypic screening to enhance genome editing. *Sci Rep* **6**, 24356.

Clijsters, L., Ogink, J. and Wolthuis, R. (2013). The spindle checkpoint, APC/C(Cdc20), and APC/C(Cdh1) play distinct roles in connecting mitosis to S phase. *J Cell Biol* **201**, 1013-26.

Courtheoux, T., Diallo, A., Damodaran, A. P., Reboutier, D., Watrin, E. and Prigent, C. (2018). Aurora A kinase activity is required to maintain an active spindle assembly checkpoint during prometaphase. *J Cell Sci* **131**.

de Groot, C. O., Hsia, J. E., Anzola, J. V., Motamedi, A., Yoon, M., Wong, Y. L., Jenkins, D., Lee, H. J., Martinez, M. B., Davis, R. L. et al. (2015). A Cell Biologist's Field Guide to Aurora Kinase Inhibitors. *Front Oncol* **5**, 285.

Dodson, C. A. and Bayliss, R. (2012). Activation of Aurora-A kinase by protein partner binding and phosphorylation are independent and synergistic. *J Biol Chem* **287**, 1150-7.

Eyers, P. A., Erikson, E., Chen, L. G. and Maller, J. L. (2003). A novel mechanism for activation of the protein kinase Aurora A. *Curr Biol* **13**, 691-7.

Floyd, S., Pines, J. and Lindon, C. (2008). APC/C Cdh1 targets aurora kinase to control reorganization of the mitotic spindle at anaphase. *Curr Biol* **18**, 1649-58.

Fuller, B. G., Lampson, M. A., Foley, E. A., Rosasco-Nitcher, S., Le, K. V., Tobelmann, P., Brautigan, D. L., Stukenberg, P. T. and Kapoor, T. M. (2008). Midzone activation of aurora B in anaphase produces an intracellular phosphorylation gradient. *Nature* **453**, 1132-6.
Giubettini, M., Asteriti, I. A., Scrofani, J., De Luca, M., Lindon, C., Lavia, P. and Guarguaglini, G. (2011). Control of Aurora-A stability through interaction with TPX2. *J Cell Sci* **124**, 113-22.
Grant, R., Abdelbaki, A., Bertoldi, A., Gavilan, M. P., Mansfeld, J., Glover, D. M. and Lindon, C. (2018). Constitutive regulation of mitochondrial morphology by Aurora A kinase depends on a predicted cryptic targeting sequence at the N-terminus. *Open Biol* **8**.
Hegarat, N., Smith, E., Nayak, G., Takeda, S., Eyers, P. A. and Hochegger, H. (2011). Aurora A and Aurora B jointly coordinate chromosome segregation and anaphase microtubule dynamics. *J Cell Biol* **195**, 1103-13.
Horn, S. R., Thomenius, M. J., Johnson, E. S., Freel, C. D., Wu, J. Q., Coloff, J. L., Yang, C. S., Tang, W., An, J., Ilkayeva, O. R. et al. (2011). Regulation of mitochondrial morphology by APC/CCdh1-mediated control of Drp1 stability. *Mol Biol Cell* **22**, 1207-16.
Kashatus, D. F., Lim, K. H., Brady, D. C., Pershing, N. L., Cox, A. D. and Counter, C. M. (2011). RALA and RALBP1 regulate mitochondrial fission at mitosis. *Nat Cell Biol* **13**, 1108-15.
Katayama, H., Zhou, H., Li, Q., Tatsuka, M. and Sen, S. (2001). Interaction and feedback regulation between STK15/BTAK/Aurora-A kinase and protein phosphatase 1 through mitotic cell division cycle. *J Biol Chem* **276**, 46219-24.
Kufer, T. A., Sillje, H. H., Korner, R., Gruss, O. J., Meraldi, P. and Nigg, E. A. (2002). Human TPX2 is required for targeting Aurora-A kinase to the spindle. *J Cell Biol* **158**, 617-23.
Levinson, N. M. (2018). The multifaceted allosteric regulation of Aurora kinase A. *Biochem J* **475**, 2025-2042.
Lindon, C., Grant, R. and Min, M. (2015). Ubiquitin-Mediated Degradation of Aurora Kinases. *Front Oncol* **5**, 307.
Lioutas, A. and Vernos, I. (2013). Aurora A kinase and its substrate TACC3 are required for central spindle assembly. *EMBO Rep* **14**, 829-36.
Littlepage, L. E. and Ruderman, J. V. (2002). Identification of a new APC/C recognition domain, the A box, which is required for the Cdh1-dependent destruction of the kinase Aurora-A during mitotic exit. *Genes Dev* **16**, 2274-85.
Macurek, L., Lindqvist, A., Lim, D., Lampson, M. A., Klompmaker, R., Freire, R., Clouin, C., Taylor, S. S., Yaffe, M. B. and Medema, R. H. (2008). Polo-like kinase-1 is activated by aurora A to promote checkpoint recovery. *Nature* **455**, 119-23.
Min, M., Mayor, U., Dittmar, G. and Lindon, C. (2014). Using in vivo biotinylated ubiquitin to describe a mitotic exit ubiquitome from human cells. *Mol Cell Proteomics* **13**, 2411-25.
Min, M., Mevissen, T. E., De Luca, M., Komander, D. and Lindon, C. (2015). Efficient APC/C substrate degradation in cells undergoing mitotic exit depends on K11 ubiquitin linkages. *Mol Biol Cell* **26**, 4325-32.
Mitra, K., Wunder, C., Roysam, B., Lin, G. and Lippincott-Schwartz, J. (2009). A hyperfused mitochondrial state achieved at G1-S regulates cyclin E buildup and entry into S phase. *Proc Natl Acad Sci U S A* **106**, 11960-5.
Nikonova, A. S., Astsaturov, I., Serebriiskii, I. G., Dunbrack, R. L., Jr. and Golemis, E. A. (2013). Aurora A kinase (AURKA) in normal and pathological cell division. *Cell Mol Life Sci* **70**, 661-87.
Otto, T., Horn, S., Brockmann, M., Eilers, U., Schuttrumpf, L., Popov, N., Kenney, A. M., Schulte, J. H., Beijersbergen, R., Christiansen, H. et al. (2009). Stabilization of N-Myc is a critical function of Aurora A in human neuroblastoma. *Cancer Cell* **15**, 67-78.
Peng, J. Y., Lin, C. C., Chen, Y. J., Kao, L. S., Liu, Y. C., Chou, C. C., Huang, Y. H., Chang, F. R., Wu, Y. C., Tsai, Y. S. et al. (2011). Automatic morphological subtyping reveals new roles of caspases in mitochondrial dynamics. *PLoS Comput Biol* **7**, e1002212.
Piljic, A., de Diego, I., Wilmanns, M. and Schultz, C. (2011). Rapid development of genetically encoded FRET reporters. *ACS Chem Biol* **6**, 685-91.

Pines, J. (2011). Cubism and the cell cycle: the many faces of the APC/C. *Nat Rev Mol Cell Biol* **12**, 427-38.
Plotnikova, O. V., Nikonova, A. S., Loskutov, Y. V., Kozyulina, P. Y., Pugacheva, E. N. and Golemis, E. A. (2012). Calmodulin activation of Aurora-A kinase (AURKA) is required during ciliary disassembly and in mitosis. *Mol Biol Cell* **23**, 2658-70.
Reboutier, D., Benaud, C. and Prigent, C. (2015). Aurora A's Functions During Mitotic Exit: The Guess Who Game. *Front Oncol* **5**, 290.
Reboutier, D., Troadec, M. B., Cremet, J. Y., Chauvin, L., Guen, V., Salaun, P. and Prigent, C. (2013). Aurora A is involved in central spindle assembly through phosphorylation of Ser 19 in P150Glued. *J Cell Biol* **201**, 65-79.
Reboutier, D., Troadec, M. B., Cremet, J. Y., Fukasawa, K. and Prigent, C. (2012). Nucleophosmin/B23 activates Aurora A at the centrosome through phosphorylation of serine 89. *J Cell Biol* **197**, 19-26.
Ruff, E. F., Muretta, J. M., Thompson, A. R., Lake, E. W., Cyphers, S., Albanese, S. K., Hanson, S. M., Behr, J. M., Thomas, D. D., Chodera, J. D. et al. (2018). A dynamic mechanism for allosteric activation of Aurora kinase A by activation loop phosphorylation. *Elife* **7**.
Salazar-Roa, M. and Malumbres, M. (2017). Fueling the Cell Division Cycle. *Trends Cell Biol* **27**, 69-81.
Scott, I. and Youle, R. J. (2010). Mitochondrial fission and fusion. *Essays Biochem* **47**, 85-98.
Seki, A., Coppinger, J. A., Jang, C. Y., Yates, J. R. and Fang, G. (2008). Bora and the kinase Aurora a cooperatively activate the kinase Plk1 and control mitotic entry. *Science* **320**, 1655-8.
Shah, K. N., Bhatt, R., Rotow, J., Rohrberg, J., Olivas, V., Wang, V. E., Hemmati, G., Martins, M. M., Maynard, A., Kuhn, J. et al. (2019). Aurora kinase A drives the evolution of resistance to third-generation EGFR inhibitors in lung cancer. *Nat Med* **25**, 111-118.
Singh, S. A., Winter, D., Kirchner, M., Chauhan, R., Ahmed, S., Ozlu, N., Tzur, A., Steen, J. A. and Steen, H. (2014). Co-regulation proteomics reveals substrates and mechanisms of APC/C-dependent degradation. *EMBO J* **33**, 385-99.
Stewart, S. and Fang, G. (2005). Anaphase-promoting complex/cyclosome controls the stability of TPX2 during mitotic exit. *Mol Cell Biol* **25**, 10516-27.
Taguchi, S., Honda, K., Sugiura, K., Yamaguchi, A., Furukawa, K. and Urano, T. (2002). Degradation of human Aurora-A protein kinase is mediated by hCdh1. *FEBS Lett* **519**, 59-65.
Tsai, M. Y., Wiese, C., Cao, K., Martin, O., Donovan, P., Ruderman, J., Prigent, C. and Zheng, Y. (2003). A Ran signalling pathway mediated by the mitotic kinase Aurora A in spindle assembly. *Nat Cell Biol* **5**, 242-8.
Violin, J. D., Zhang, J., Tsien, R. Y. and Newton, A. C. (2003). A genetically encoded fluorescent reporter reveals oscillatory phosphorylation by protein kinase C. *J Cell Biol* **161**, 899-909.
Zeng, K., Bastos, R. N., Barr, F. A. and Gruneberg, U. (2010). Protein phosphatase 6 regulates mitotic spindle formation by controlling the T-loop phosphorylation state of Aurora A bound to its activator TPX2. *J Cell Biol* **191**, 1315-32.
Zorba, A., Buosi, V., Kutter, S., Kern, N., Pontiggia, F., Cho, Y. J. and Kern, D. (2014). Molecular mechanism of Aurora A kinase autophosphorylation and its allosteric activation by TPX2. *Elife* **3**, e02667.

Figures

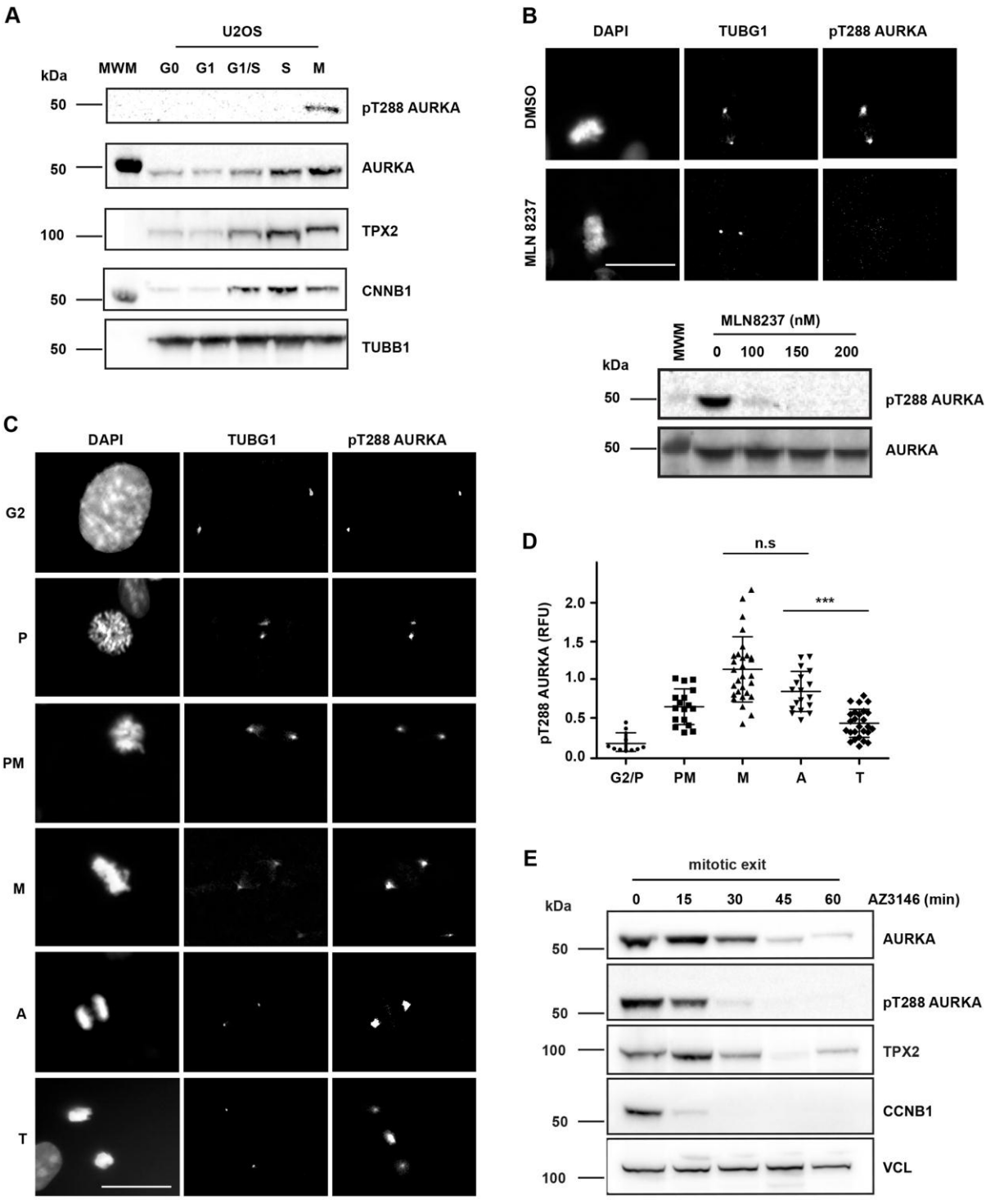

Figure 1: Inactivation of AURKA during mitotic exit begins at anaphase

A pT288 antibody detects active AURKA only in mitotic cells. Cells were synchronized as described in Materials and Methods and blotted for pT288, total AURKA and other mitotic

markers. **B** pT288 signal is sensitive to AURKA-specific inhibitor MLN8237 by IF on mitotic cells from a MeOH-fixed unsynchronized population (upper panel) or by immunoblot of STLC-arrested mitotic cells treated for 3 hours at the indicated doses (lower panel). AURKA-specific pT288 signal is restricted to centrosomes and spindle pole bodies (marked by γ-tubulin, TUBG1). Bars, 10 μm. See also Figure S1. **C - E** Quantification of pT288-AURKA during mitotic exit. **C, D** Unsynchronized cell populations were fixed and stained as in **B**. Cells were judged to be at different stages of mitosis according to DAPI staining (**C**) and scored for mean pT288 AURKA signal measured in a fixed ROI centred on TUBG1 signal at centrosomes or spindle poles (**D**). Scatter plots show distribution, means ± S.D. of pooled data from two independent experiments. Data are normalized to mean value in each category. The plot is representative of two biological replicates. G2 and prophase (P), n=10; prometaphase (PM), n=15; metaphase (M), n=30; anaphase (A), n=30; and telophase (T), n=26. M vs A, not significant (n.s.); A vs T, $p < 0.0001$ (***), Students' t-test. RFU, Relative Fluorescence Units. **E** Cells were synchronized in 5 μM STLC and released by checkpoint inhibition using 10 μM AZ3146, with extracts harvested at times indicated. These were examined by immunoblotting for AURKA, pT288-AURKA and TPX2 levels. Disappearance of Cyclin B1 (CCNB1) acts as marker for mitotic exit, level of vinculin (VCL) as loading control.

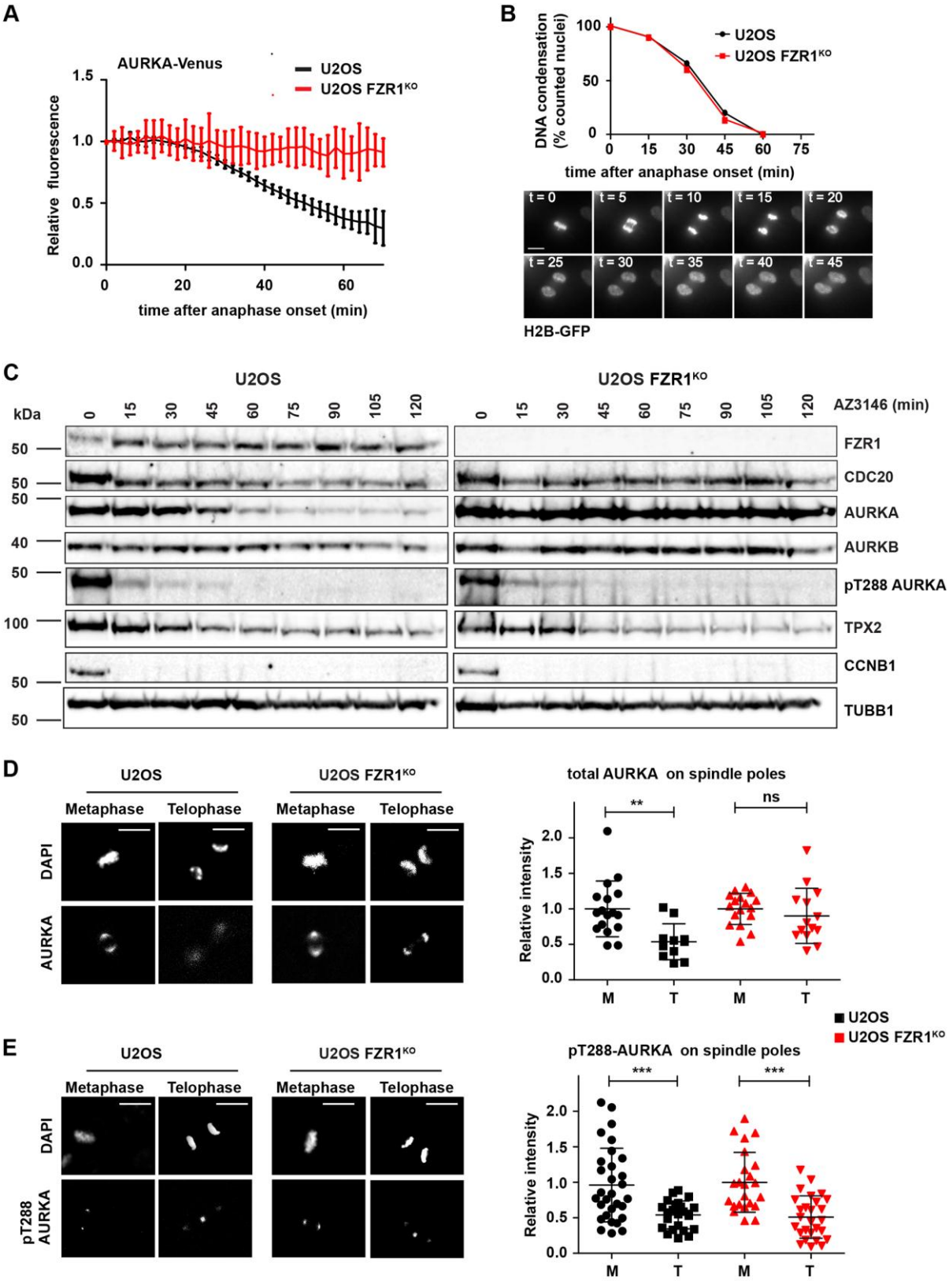

Figure 2: AURKA destruction is not required for pT288-AURKA down-regulation at mitotic exit

A, B There is no mitotic exit destruction of AURKA in FZR1/Cdh1 KO cells ($FZR1^{KO}$). AURKA-Venus (**A**) or H2B-GFP (**B**) was transiently transfected into both U2OS and U2OS $FZR1^{KO}$ cells. **A** Quantifications of total fluorescence measurements from single mitotic cells were used to generate degradation curves for AURKA-Venus. Fluorescence values for individual curves were normalized to the last frame before anaphase onset, and all curves *in silico* synchronized to anaphase. n = 10 cells. **B** H2B-GFP fluorescence was used to score DNA as condensed or decondensed in cells undergoing mitotic exit (example shown in lower panels). Percentage of cells with condensed DNA over time was plotted as a measure of cumulative mitotic exit. n ≥ 10 cells. **C - E** AURKA activity scored by pT288 is not affected by $FZR1^{KO}$ during mitotic exit. **C** U2OS and $FZR1^{KO}$ cells were synchronized to prometaphase using 5 µM STLC and released by checkpoint inhibition using 10 µM AZ3146, with extracts harvested at times indicated. Lysates were analyzed by immunblot with antibodies against AURKA, pT288-AURKA and other mitotic regulators. **D, E** pT288-AURKA and AURKA staining associated with individual centrosomes/spindle poles in metaphase (M) versus telophase (T) cells (lefthand panels). Fluorescence values were measured as in Figure 1 and are presented as scatter plots, with mean ± S.D. indicated, for total AURKA (**D**) and pT288-AURKA (**E**) in both U2OS and $FZR1^{KO}$. All values were normalized to the mean value from control metaphase cells. ns, non-significant; ** $p < 0.001$; *** $p < 0.0001$, Student's t-test. **D**, n ≥ 11 from one experiment; **E**, n ≥ 23 from two experiments. Bars, 10 µm.

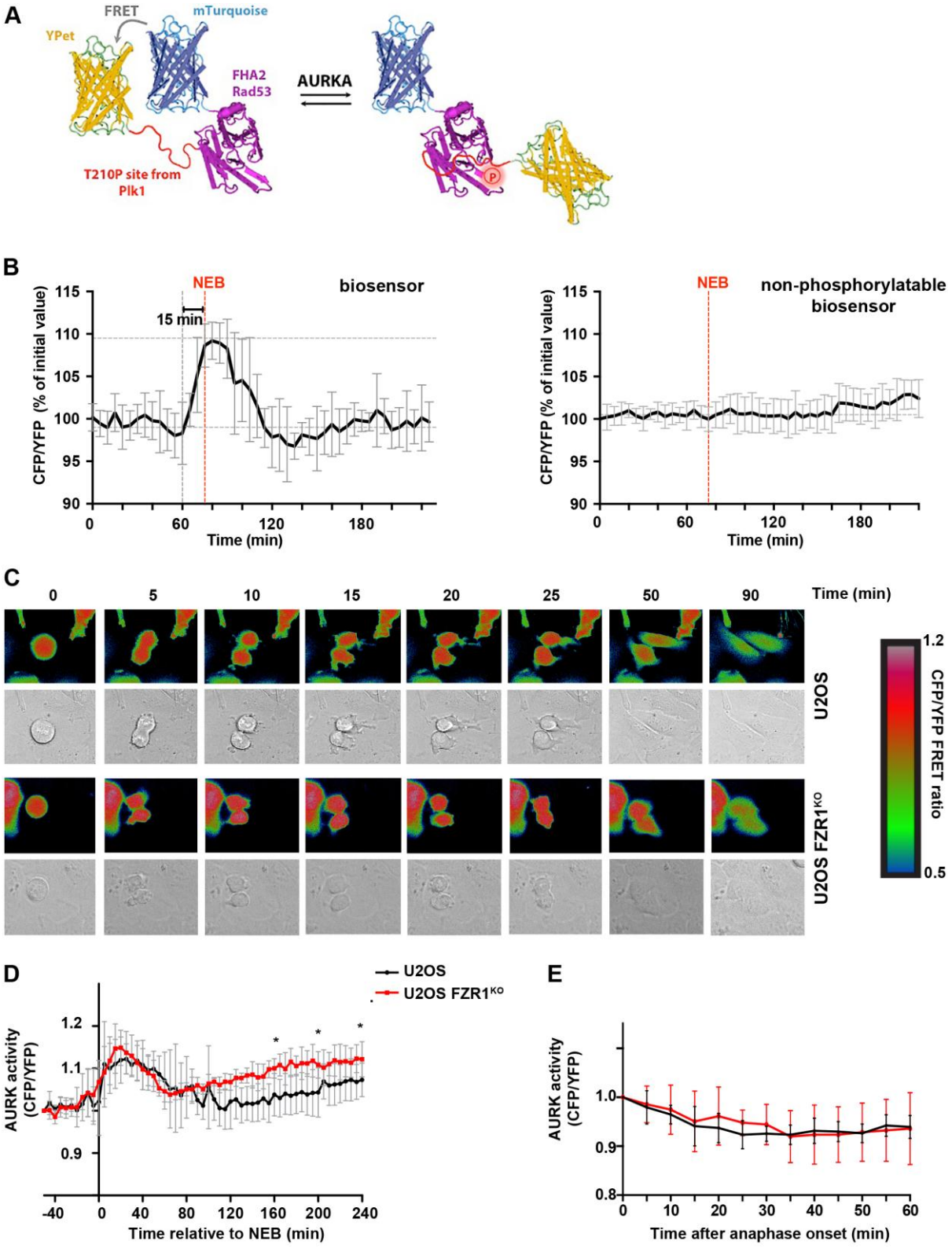

Figure 3: A FRET-based biosensor records unaltered parameters of mitotic AURKA activation and inactivation in FZR1^{KO} cells

A Schematic illustration of AURKA biosensor showing high FRET (left) versus low FRET states (right). **B** Inverted FRET measurements (CFP/YFP emission) from timelapse movies of cells expressing the biosensor, or a non-phosphorylatable version, show that the biosensor reports on mitotic phosphorylation events, n ≥ 8. Further characterization of the specificity of the biosensor is shown in Supplementary Figure S4. **C** Examples of inverted false-coloured FRET ratio of biosensor-expressing single U2OS and FZR1^{KO} cells passing through mitosis: High FRET (blue) reports on non-phosphorylated state, whereas low FRET (red) reports on the phosphorylated probe. **D, E** FRET ratio values measured using biosensor show AURK activity is normally regulated through mitosis in FZR1^{KO} cells but rises again in G1 phase (*, $p < 0.05$, Student's t-test). **D** Cells *in silico* synchronized to NEB. **E** Cells *in silico* synchronized and FRET values normalized to anaphase onset.

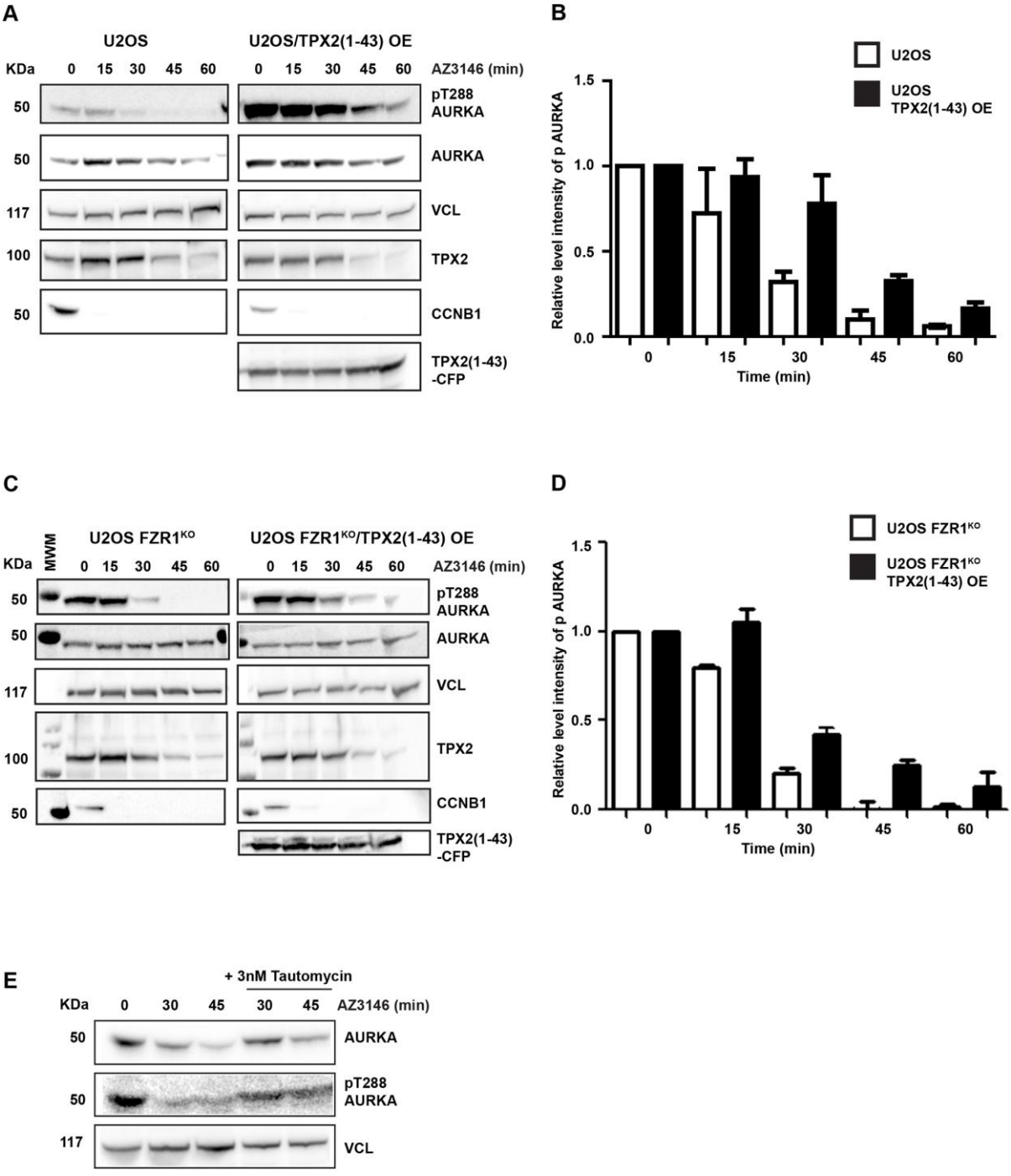

Figure 4: AURKA inactivation is controlled through TPX2.

U2OS (**A, B**) and FZR1^{KO} (**C, D**) cells were transfected with TPX2(1-43)-CFP and synchronized through mitotic exit as described in the legend to Figure 2. Quantitative immunoblotting of cell lysates shows that loss of pT288-AURKA during mitotic exit is delayed in the presence of TPX2(1-43) in both parental and FZR1^{KO} cells. Cyclin B1 (CCNB1) is used as marker for mitotic exit, level of vinculin (VCL) as loading control. Bar charts **(B, D)** show pT288 signal normalized against vinculin. Results presented are mean values from 3

independent experiments ± S.D. **E** AURKA inactivation is phosphatase-dependent. U2OS cells undergoing mitotic exit were treated with 3 nM PP1 inhibitor tautomycin 10 minutes after relief of SAC arrest by AZ3146. Lysates harvested at the indicated time points after AZ3146 treatment were subject to immunoblot analysis.

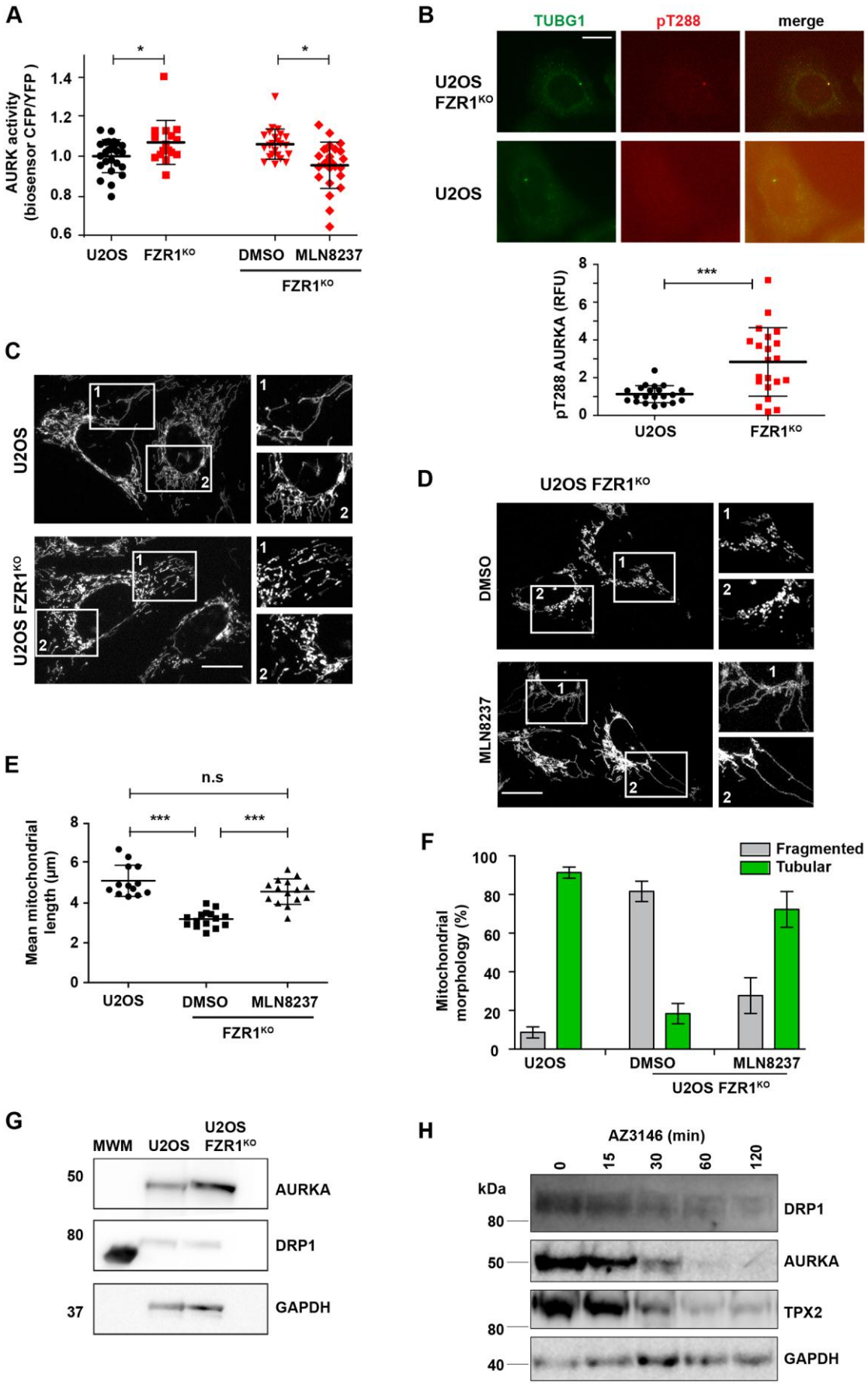

Figure 5: Destruction of AURKA by APC/C$^{Cdh1/FZR1}$ is required to control interphase activity of AURKA.

A The FRET biosensor reveals raised Aurora kinase activity in interphase FZR1^{KO} cells. Cells were synchronized in G1/S using double thymidine block, and treated (or not) for 3 hours with 100 nM AURKA inhibitor MLN8237. Scatter plots show CFP/YFP emission ratios with mean ± S.D. from individual cells in U2OS and FZR1^{KO} populations ($n = 20$; $p < 0.05$, Student's t-test) and are representative of two independent experiments. **B** pT288 staining in fixed cells synchronized at G1/S, and scatter plots of centrosomal pT288 signal quantified as in Figure 1, show that pT288 can be detected at centrosomes of G1/S FZR1^{KO} cells, but not at centrosomes of parental U2OS cells. ***, $p \leq 0.0001$, $n \geq 21$, Student's *t*-Test. RFU, Relative Fluorescence Units. **C - F** Mitochondria are over-fragmented in interphase FZR1^{KO} cells in an AURKA-sensitive manner. U2OS and FZR1^{KO} cells were synchronized in G1/S then stained with MitoTracker® and imaged live (**C**). FZR1^{KO} cells were treated with DMSO or 100nM MLN8237 for 3 hours (**D**). Scale bars, 10 µm. **E** Quantitative analyses of fragmented mitochondria length was carried out as described in Materials and Methods and are presented as scatter plots with mean ± S.D. indicated ($n \geq 15$ cells; $p < 0.001$ by 2-tailed Mann-Whitney U test), whilst (**F**) percentages of tubular versus fragmented morphologies were calculated using MicroP software and are presented as mean values ± S.D ($n \geq 15$; $p < 0.0001$ by 2-tailed Mann-Whitney U test). **G, H** Immunoblotting U2OS and FZR1^{KO} cells shows that DRP1 levels, unlike those of AURKA, are not altered in G1/S FZR1^{KO} cells (**G**), even though DRP1 undergoes modest degradation during mitotic exit (**H**).

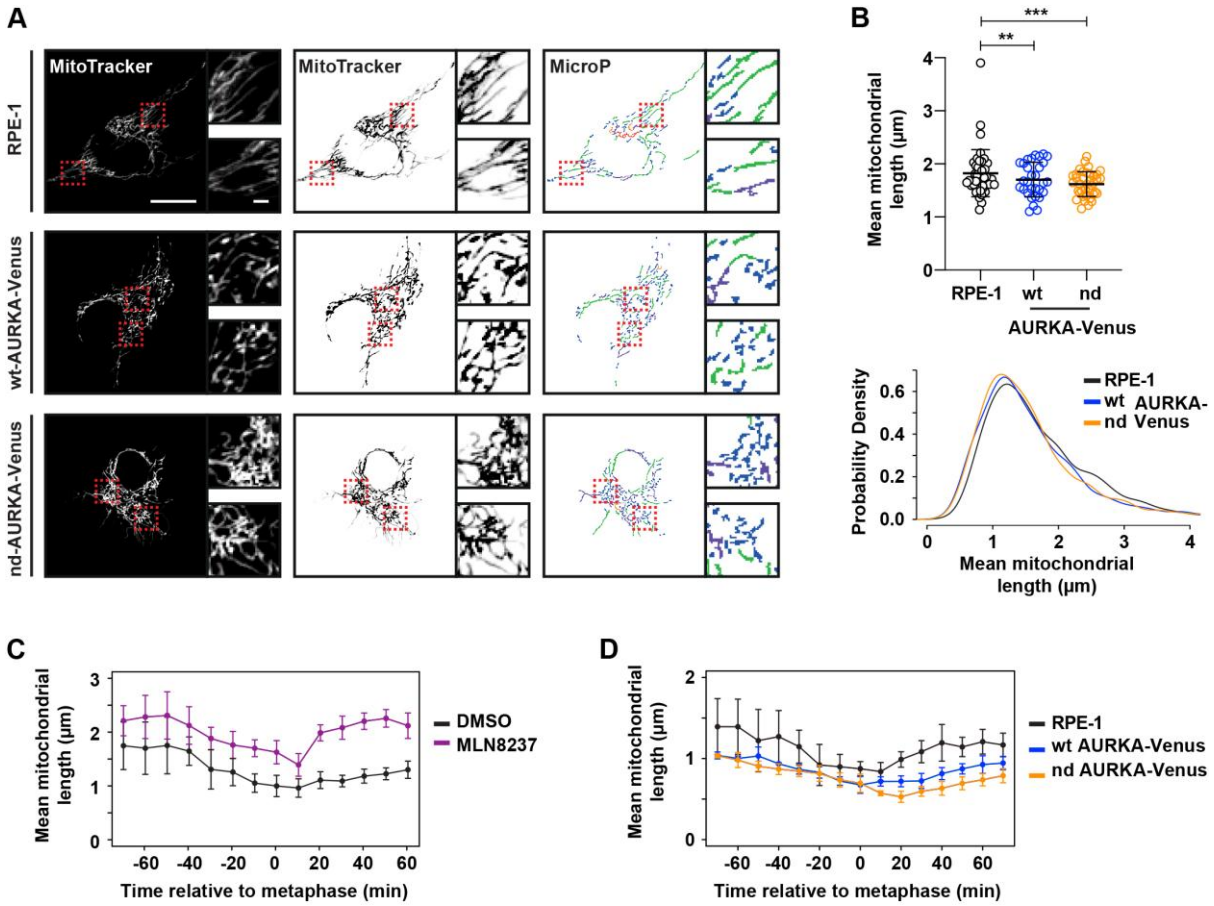

Figure 6: Undegraded AURKA at mitotic exit inhibits reassembly of the interphase mitochondrial network.

A, B RPE-1, RPE-1 AURKA-Venus-WT and non-degradable version (nd, Δ32-66) cell lines were stained with MitoTracker® and imaged 24 h after induction of AURKA transgene expression. Acquired images were analysed with MicroP (**A**) and subjected to mitochondria length quantifications (**B**). Scatter plots show mean ± S.D. for mean mitochondrial lengths from 30 mitochondria per cell in 18-24 cells per condition from two experimental replicates (upper panel). p-values are calculated from raw measurements using Mann-Whitney test: **, $p < 0.001$; ***, $p < 0.0001$; $n \geq 600$. Lower panel shows Kernel density plots of raw data. **C** RPE1 cells treated with either DMSO or 100 nM MLN8237 were stained with MitoTracker® and filmed live as they progressed through mitosis. Mean mitochondrial length over time is plotted for $n \geq 6$ cells per condition in two experimental replicates. **D** RPE-1 AURKA-Venus-WT and -nd cells were stained with MitoTracker®, filmed and analysed as in C, $n \geq 5$ cells.

SUPPLEMENTARY FIGURES

AURKA destruction is decoupled from its activity at mitotic exit but essential to suppress interphase activity.
Abdelbaki et al.

Figure S1

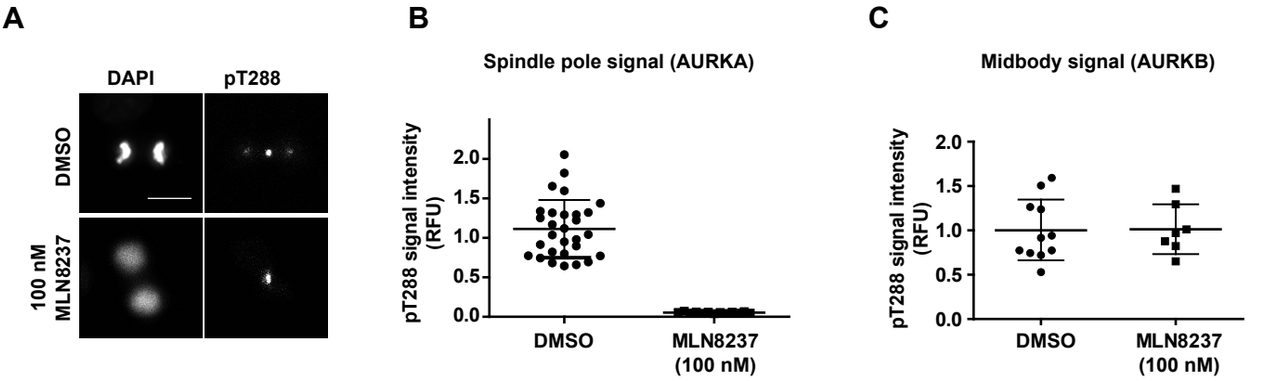

Figure S1: Specificity of pT288-AURKA signal in mitotic cells. Immunofluorescence analysis of mitotic U2OS cells fixed and stained with antibody against pT288-AURKA shows signal at both spindle poles and midbody (**A**). pT288 signal at spindle poles and midbody was measured in cells treated for 3 hours prior to fixation with 100 nM AURKA inhibitor MLN8237 or DMSO control (**B**, **C**). Spindle pole signal was ablated following MLN8237 treatment and is therefore specific for AURKA activity (**B**) whereas midbody signal is refractory to MLN8237 inhibition and attributed to recognition of pT232-AURKB epitope (**C**). Scatter plots show distributions with mean ± S.D. of pT288 signal intensity measurements expressed as background-corrected mean pixel values in a ROI at spindle pole or midbody, normalized to the mean value of the control (DMSO-treated) population. RFU, Relative Fluorescence Units. Size bar, 10 μM.

Figure S2

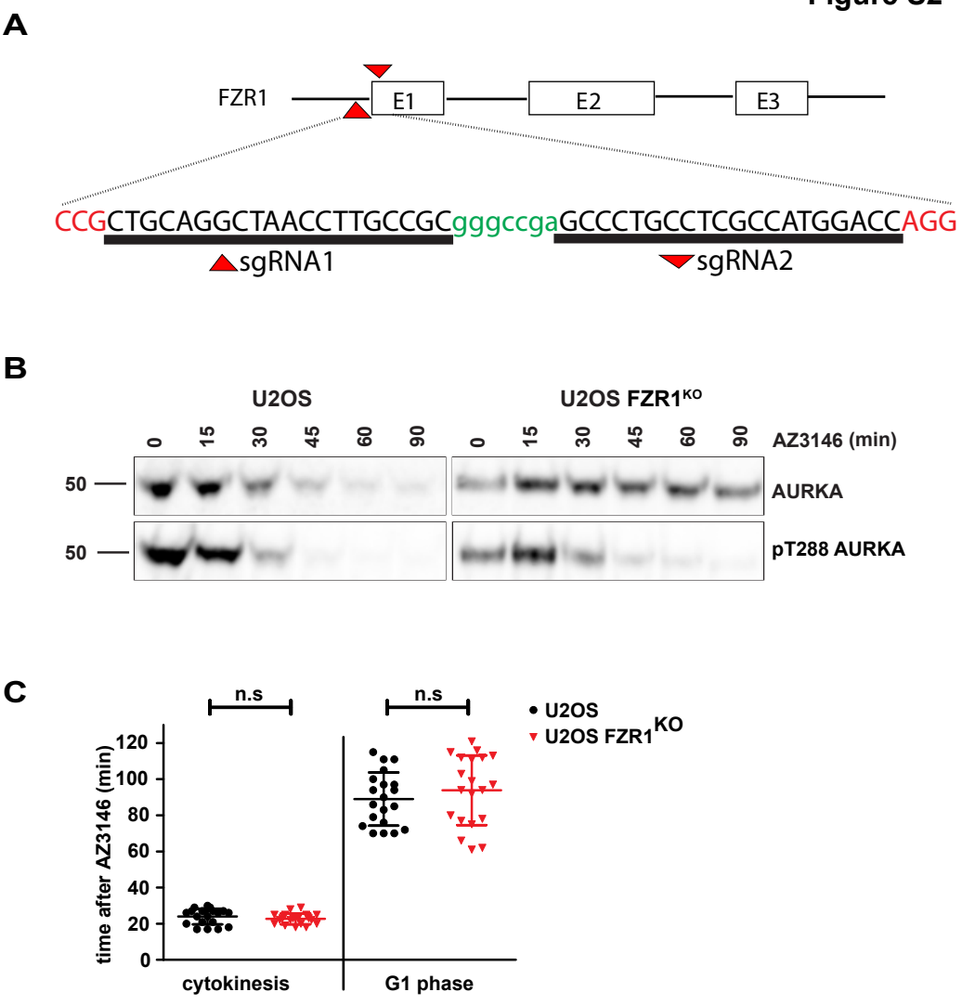

Figure S2: Regulation of AURKA during mitotic exit in FZR1^{KO} cells. A Schematic showing guide RNAs used to generate CRISPR/Cas9 knockout of FZR1. **B** Dynamics of AURKA degradation and inactivation in a second clone of FZR1^{KO} cells. Extracts were prepared and processed as in Figure 2C and blotted with the antibodies indicated. **C** Kinetics of forced mitotic exit in parental U2OS and FZR1^{KO} cells. Cells synchronized according to the protocol used for Figure 2C immunoblots were pre-incubated for one hour with 10uM sir-DNA, then filmed by timelapse microscopy to score cells for cytokinesis timing (onset of cortical contractility) and return to interphase (decondensed chromosomes, nuclear envelope reformed, cells adhered).

Figure S3

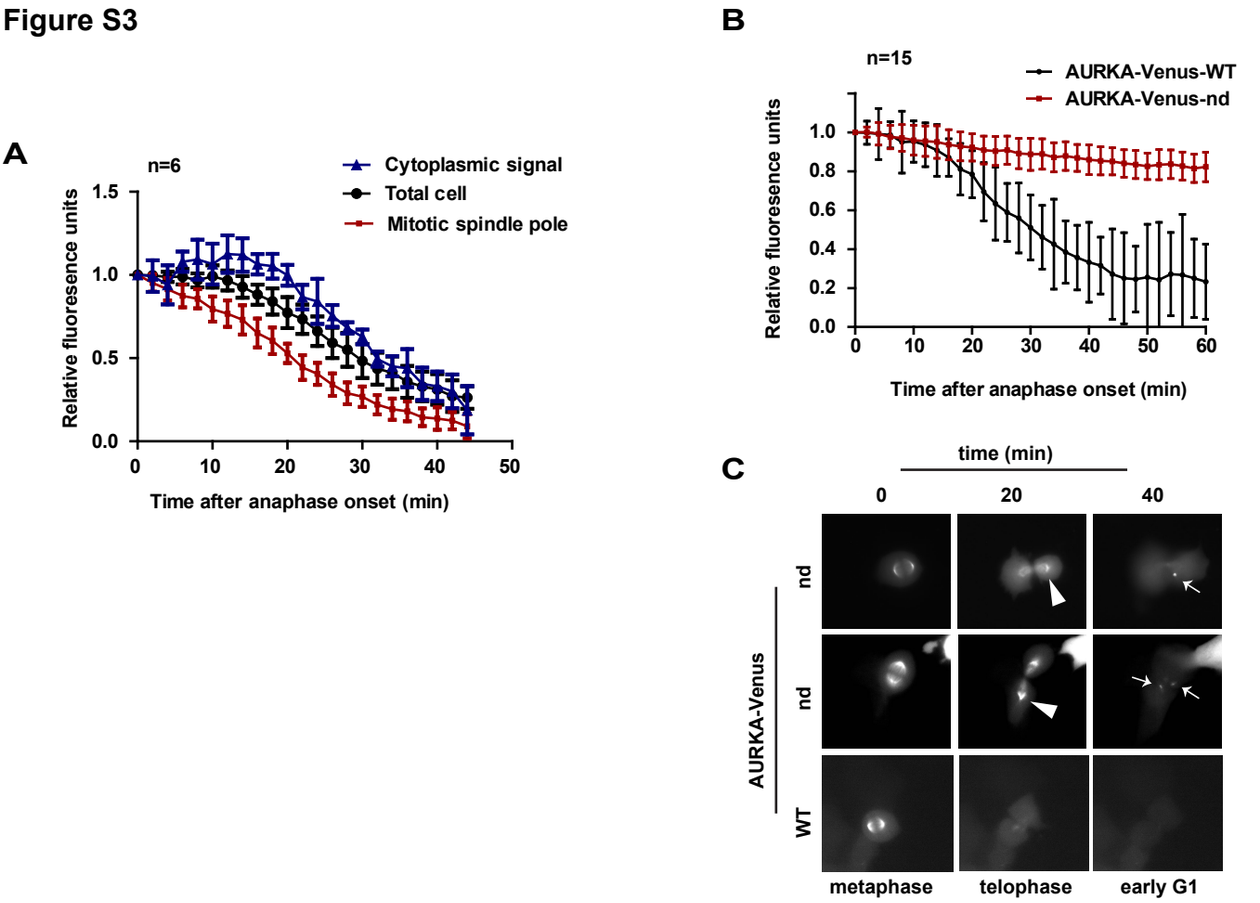

Figure S3: FZR1-dependent degradation of AURKA at spindle poles. A-C Undegraded AURKA persists at spindle poles: RPE-1 FRT/TO cells expressing tet-inducible wild-type (WT) or non-degradable (Δ33-64, nd) AURKA-Venus were subjected to timelapse fluorescence imaging during mitosis, and fluorescence levels quantified as readout for mitotic exit degradation of AURKA. **A** Separate quantification on spindle poles and in the cytoplasm shows robust loss of AURKA-Venus-WT from spindle poles correlates with degradation of the protein (loss of total cell signal), n ≥ 6. **B** AURKA-Venus-nd is stable during the mitotic exit window when WT-AURKA-Venus is degraded (n ≥ 15) and (**C**) remains strongly associated with spindle poles in telophase (arrowheads). **C** AURKA-Venus-nd can still be detected at centrosomes in early G1 phase (arrows), at a time when AURKA-Venus-WT is no longer detectable.

Figure S4

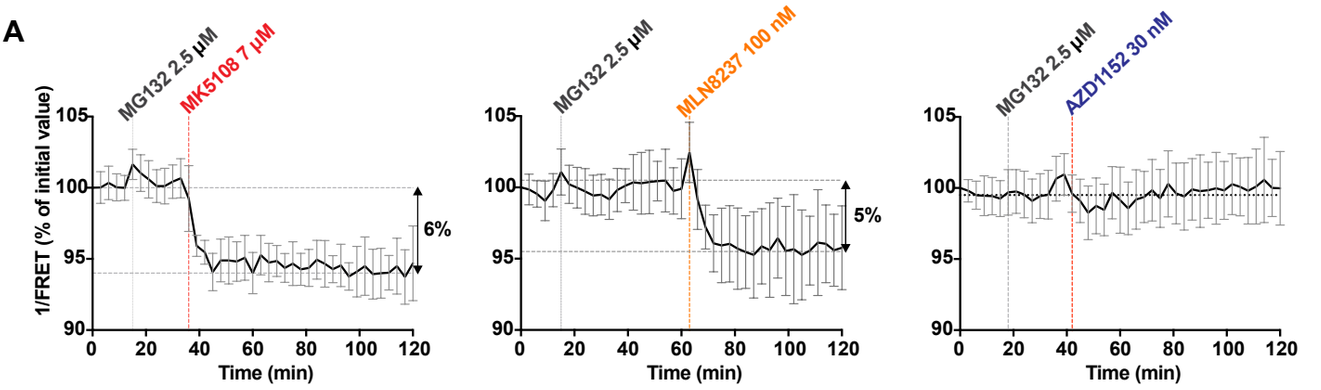

	[inhibitor]	mitotic activity inhibition	number of cells analysed
AURKA inhibitor	MK5108 7 µM	6%	13
	MLN8237 200 nM	6%	16
	MLN8237 100 nM	5%	13
AURKB inhibitor	ZM447439 2 µM	2%	12
	AZD1152 500 nM	2%	22
	AZD1152 30 nM	< 1%	18

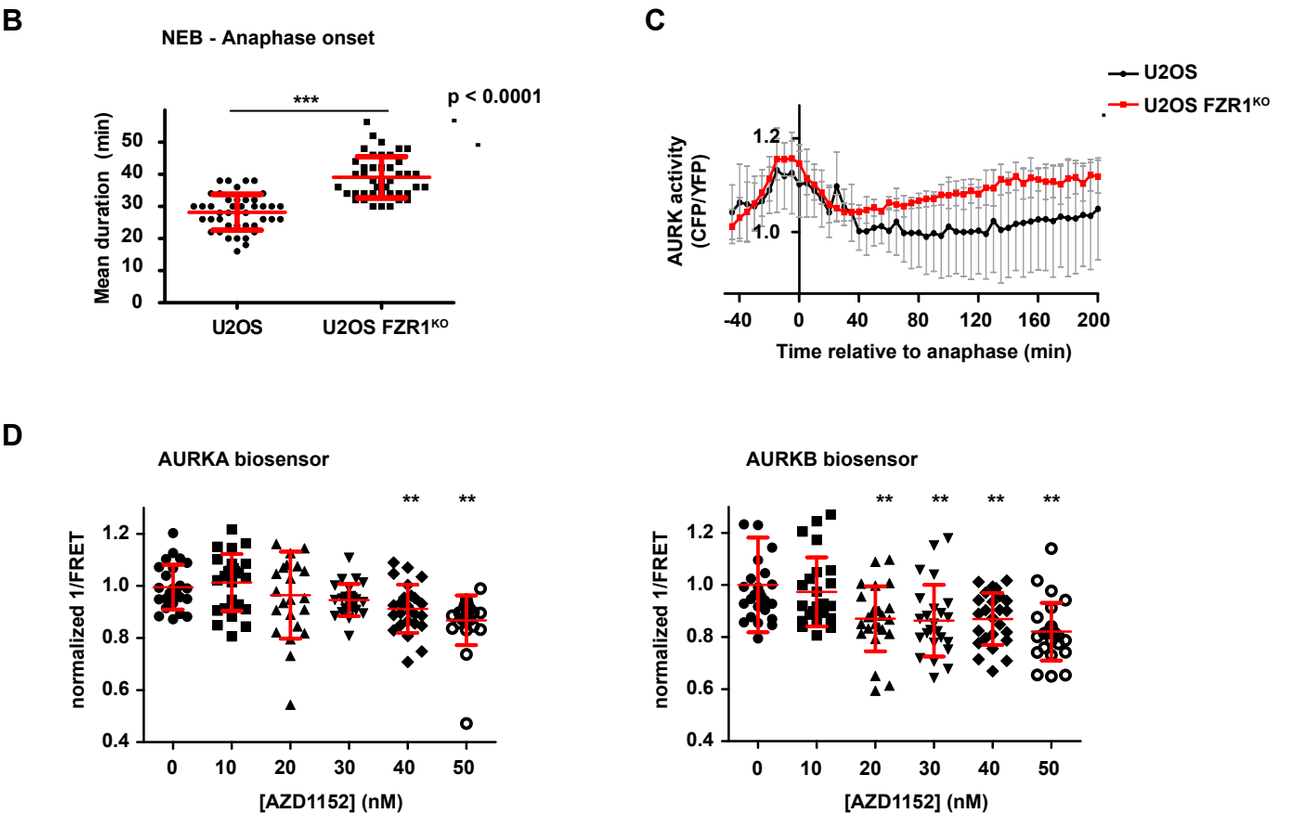

Figure S4: Measuring Aurora kinase activity with a FRET-based biosensor.

A U2OS cells transfected with the AURKA-directed biosensor from a population synchronized by release from double thymidine block were arrested in mitosis by treatment with MG132, then treated with AURKA- or AURKB-specific inhibitors. Mean activity values (1/FRET) for mitotic cells

undergoing different drug treatments are shown in the traces (upper panels) and results from a number of different experiments summarized in the table below. Biosensor activity was strongly inhibited by treatment with MLN8237 or MK5108, specific inhibitors of AURKA, and partially inhibited by two inhibitors of AURKB, AZD1152 and ZM447439. **B** Mitotic exit is delayed by approximately 10 min in $FZR1^{KO}$ cells. Times from NEB to anaphase in individual cells are shown as scatter plots with mean values ± S.D., n > 40, $p < 0.001$ by Students *t*-test. **C** AURKA-directed biosensor activity (data from Figure 3D) *in silico* synchronized to anaphase onset to take account of different timings shown in **B**. **D** Activity of AURKA-directed biosensor in interphase $FZR1^{KO}$ cells is insensitive to 30 nM dose of AZD1152 that is sufficient to inhibit activity of an AURKB-directed sensor. FZR1KO cells were arrested at G1/S by application of double thymidine block and treated for 3 hours with AZD1152 at indicated doses. 1/FRET values calculated for individual cells and normalized against the population mean are shown as scatter plots with mean ± S.D. indicated foreach condition. **, $p < 0.001$, Mann-Whitney U-test.

Figure S5

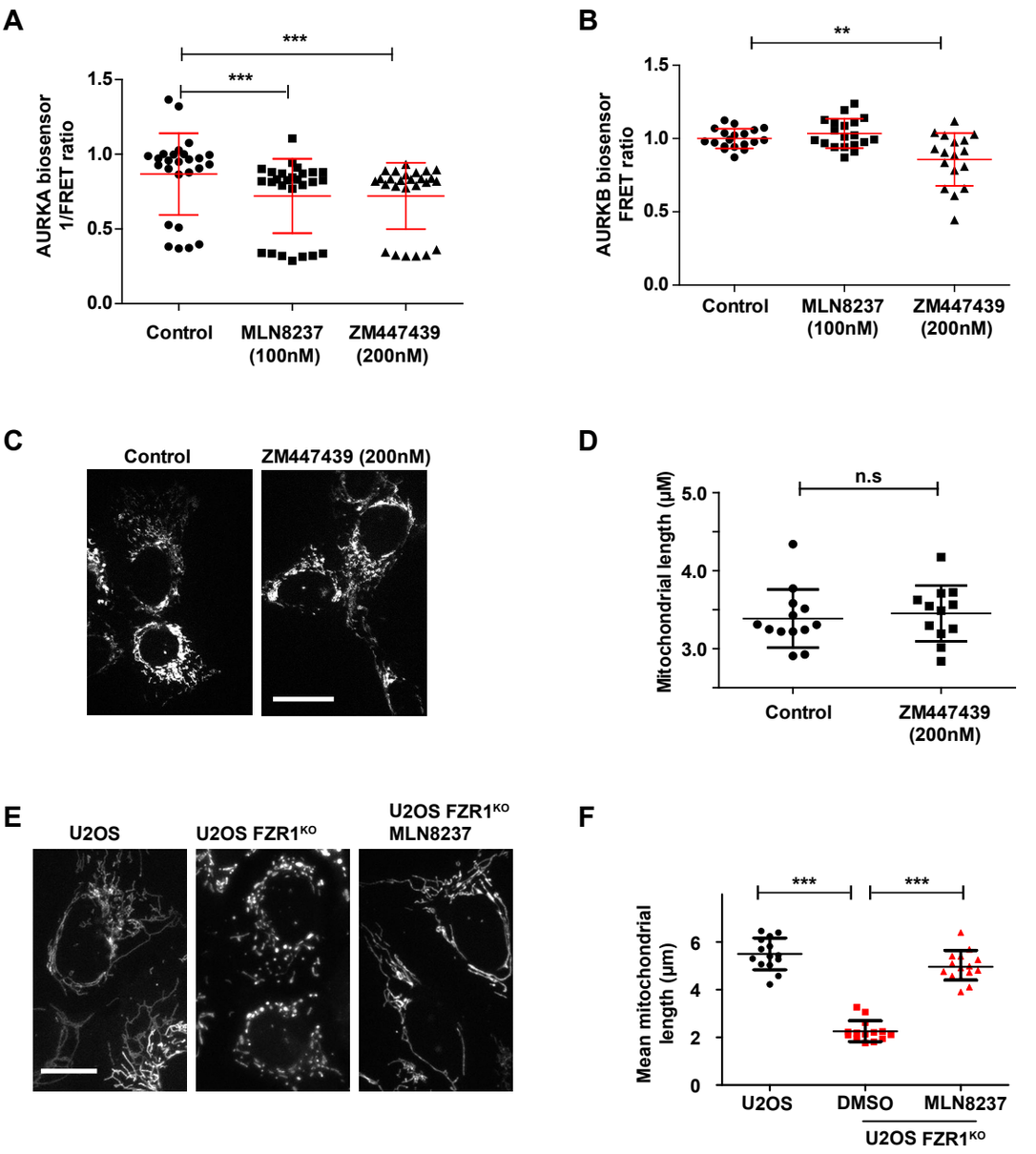

Figure S5: Regulation of mitochondrial fragmentation in FZR1^{KO} cells depends on AURKA. **A-B** FZR1^{KO} cells transfected with either AURKA- or AURKB-directed cytoplasmic biosensors were synchronized at the G1/S boundary as in Figure 4 and challenged for 3 hours with AURKA-specific inhibitor MLN8237 or AURKB-specific inhibitor ZM447439 at the indicated doses. FRET values are presented as in Figure S4D. **A** The AURKA biosensor signal was sensitive to either inhibitor (n ≥ 25). **B** the AURKB biosensor responded to ZM447439 but was insensitive to MLN8237 (n ≥ 19) and we concluded that MLN8237 does not inhibit AURKB activity in FZR1^{KO} cells. **C, D** FZR1^{KO} cells were treated with 200 nM ZM447439 for 3 hours then stained with MitoTracker® for measurement of mitochondrial fragment lengths. AURKB inhibition had no effect on mitochondrial fragmentation, as illustrated in representative panels shown in **C,** and in scatter plots (**D**) expressed as means of 30 mitochondrial fragment lengths per cell, n ≥ 13. **, $p < 0.01$; ***, $p < 0.001$; n.s. non-significant, by Mann-Whitney U-test. **E, F** AURKA activity-dependent fragmentation of mitochondria in a second FZR1^{KO} clone. Mitochondrial lengths were quantified in a replicate of the experiment shown in Figure 5E. ***, $p < 0.001$ by Mann-Whitney U-test.

Figure S6

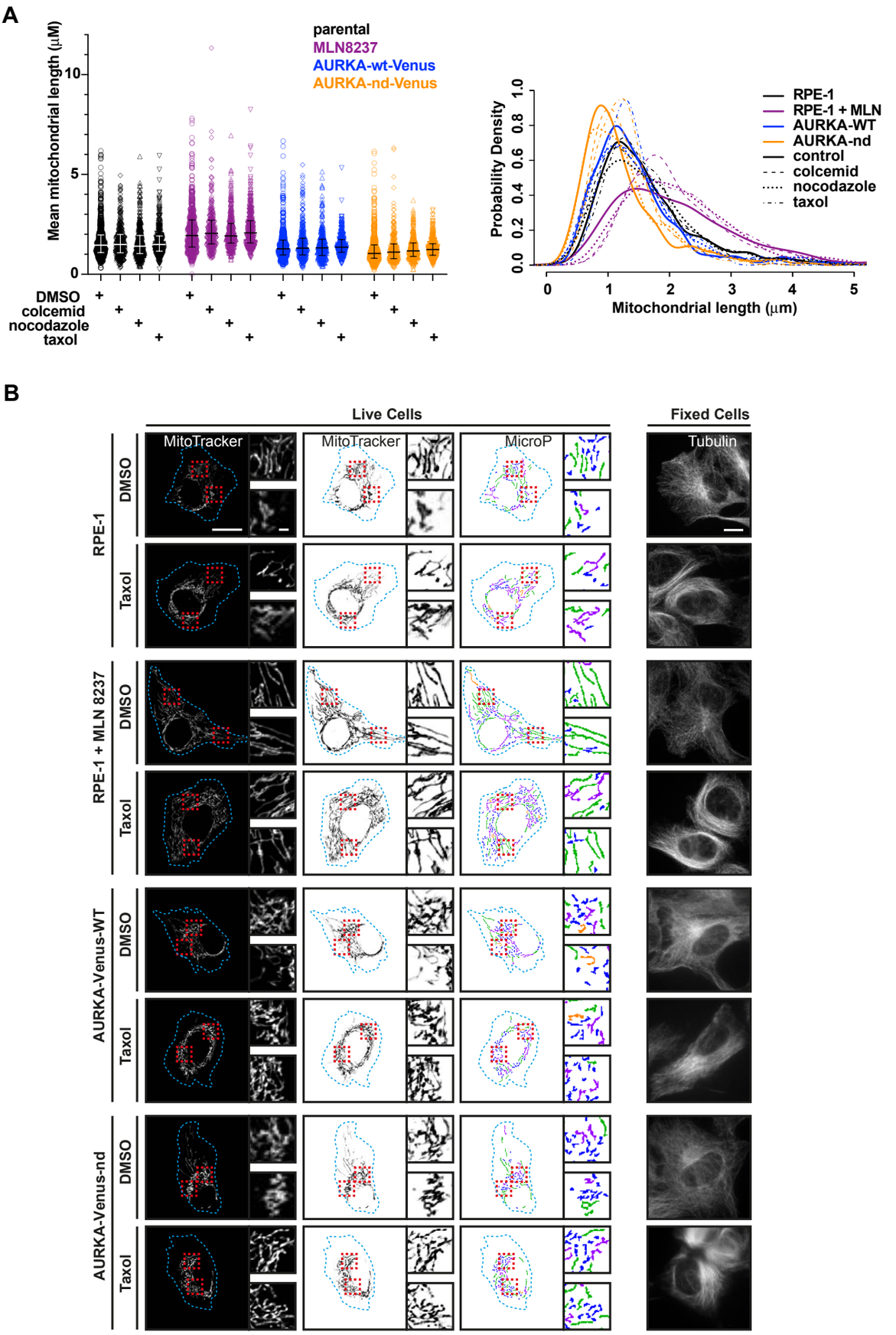

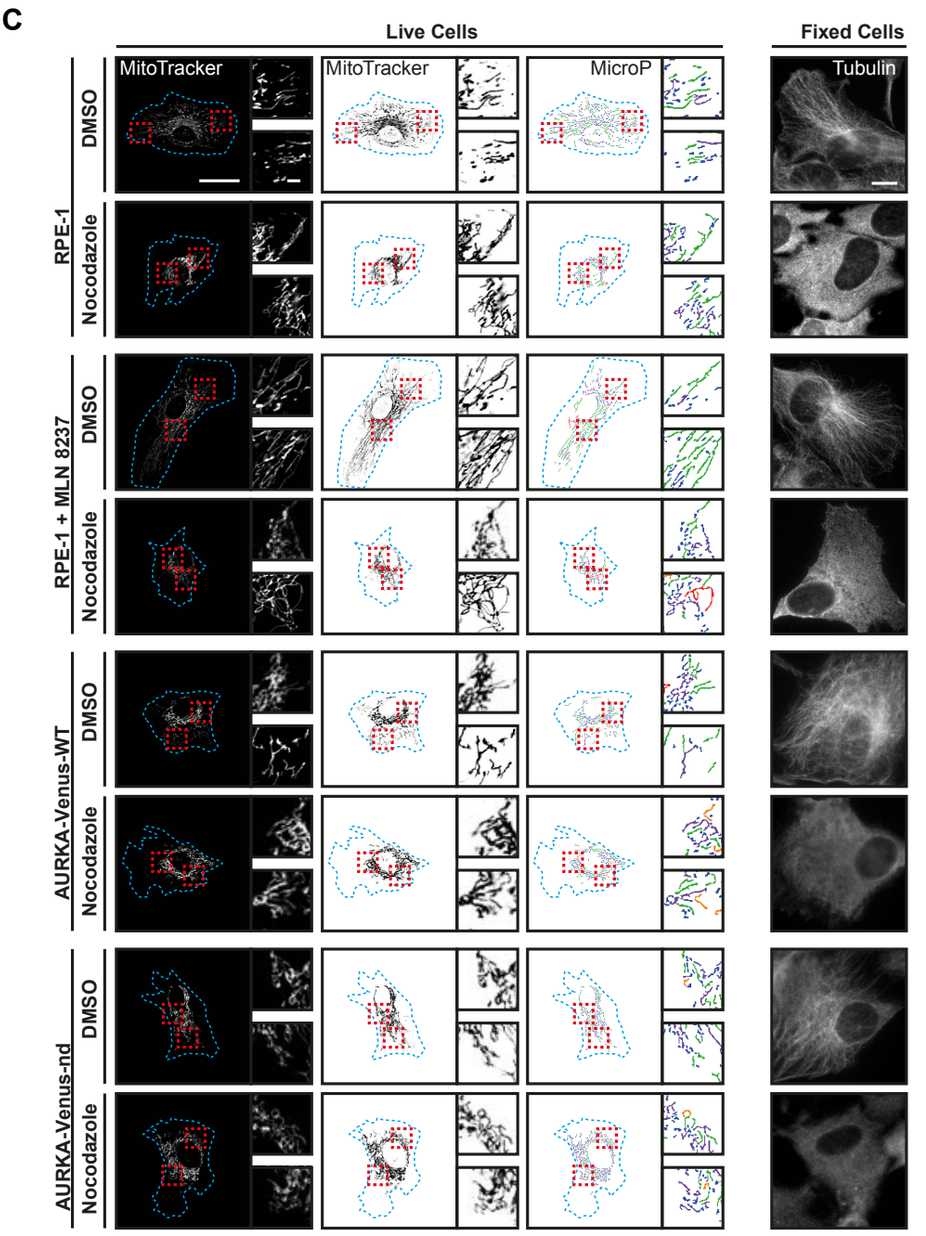

Figure S6: Altered mitochondrial dynamics in response to AURKA are independent of microtubule dynamics. Parental RPE-1 cells (± 100 nM MLN8237 treatment, 3 hours) and cell lines induced for expression of WT- and nd- AURKA-Venus for 24 h were treated for 30 min with 1.5 μM colcemid or 500 ng/ml nocodazole, or for 60 min with 5 μM taxol. Cells were then either stained with MitoTracker® for live imaging of mitochondria (**A-C**) or fixed and stained for microtubules with an antibody against β-tubulin (**B-C**). **A** Scatter plots of individual mitochondrial lengths (30 mitochondria/ cell, n≥ 20 cells per condition) with mean ± S.D. indicated (left hand panel) or as kernel density plots to show size distribution (right hand panel). *p*-values within each set DMSO/colcemid/nocodazole/taxol = n.s.; *p*-value between sets (DMSO treatment in parental/MLN-treated/AURKA-wt/AURKA-nd) < 0.0001 (One-way Anova). **B-C** Illustrative panels

of cells treated with taxol (**B**) or nocodazole (**C**). From left to right in each set of panels: Image of MitoTracker-stained cell with magnified inserts, inverted image for enhanced visualization of mitochondria with magnified inserts, MicroP analysis of MitoTracker staining with magnified inserts, immunofluorescence detection of microtubules in a methanol-fixed cell from a population treated in parallel with the same drugs. MicroP colour code for mitochondrial morphology: blue, small globular; green, simple tubular; purple, branching tubular; orange, twisting tubular; red, donuts, loops and non-resolvable segments.